Title

Tyrosine-sulfated peptide-induced flavonol biosynthesis controls elongation and differentiation in Arabidopsis primary root

Journal

The Plant Cell, 38(7)

ISSN

1040-4651

Authors

Ercoli, Maria Florencia
Shigenaga, Alexandra M
Teixeira de Araujo, Artur
et al.

Publication Date

2026-06-16

DOI

10.1093/plcell/koag180

Note: The snapshot PDF is a proof copy of the corrections marked in nEdit, the layout will be different from a typeset PDF and the view of the article in nEdit.

Author Queries/Comments

AQ0 : Please follow the link below to review, edit, or add to suggested topic values for your paper. Please confirm when you have completed this step. To access the DIVE site, click here.
Response: Completed

AQ1 : Please note that any email and address details visible on this proof will be published. If you do not have an institutional email or address, and a personal email/home address has been included on these proofs, please indicate if you would prefer for these to be removed. In such cases we will publish the city and country in place of a full address.
Response: Resolved

AQ2 : Please check the spelling and accuracy of all author names and affiliations, particularly for any co-authors. Also check that author surnames are correctly highlighted. This is to ensure that forenames and surnames are tagged correctly for online indexing. Incorrect names and affiliations may lead to an author not being credited for their work by funders, institutions, or other third parties. Make any changes directly in the text.
Note that changes to your authorship list (adding or removing authors, changing designation of corresponding author) require additional approvals. Email journals.corrections@oup.com if this is required.
Response: All first and last names have been confirmed. Please add ORCID to author Alexandra M. Shigenaga https://orcid.org/0000-0001-8649-2891

AQ3 : Please provide country for affiliation 1 directly in the text.
Response: Resolved

AQ4 : Please provide country for affiliation 2 directly in the text.
Response: Resolved

AQ5 : Please provide country for affiliation 3 directly in the text.
Response: Resolved

AQ6 : Please provide country for affiliation 4 directly in the text.
Response: Resolved

AQ7 : Please provide country for affiliation 5 directly in the text.
Response: Resolved

AQ8 : Please provide country for affiliation 6 directly in the text.
Response: Resolved

AQ9 : Please provide the department, institution, postal address, city, postal code, country and email for the corresponding author directly in the text.
Response: Resolved

AQ10 : If your manuscript has figures or text from other sources, please ensure you have permission from the copyright holder. Also ensure that the copyright owner is properly credited, for instance in the figure legends. Make any changes directly in the text. For any questions about permissions, contact jnls.author.support@oup.com.
Response: The image was created by the first author.

AQ11 : Please note that the provided URL (https://david.ncifcrf.gov/) is not valid/accessible in text. Check and include a working URL directly in the text.
Response: the updated URL is https://davidbioinformatics.nih.gov

AQ12 : Please check that funding is recorded in a separate funding section, if applicable. Use the full official names of any funding bodies and include any grant numbers. Insert any changes to the funding section directly in the text.
Response: Resolved

AQ13 : The grant sponsor name “Joint Bioenergy Institute” that you have provided is not available in the CrossRef funder-

registry (see https://www.crossref.org/services/funder-registry/). Please check the grant sponsor name is correct, make any changes directly in the text.
Response: The funder for the Joint Bioenergy Institute is the US Department of Energy. I corrected the text to reflect that.

AQ14 : Please ensure all “conflicts of interest” (or “disclosures”) have been included for you and your co-authors, and that this section is correct. Edit the text directly if changes are required.
Response: Resolved

AQ15 : Missing details have been imported to the references from PubMed/CrossRef. Please check and, if necessary, edit the references directly.
Response: Resolved

AQ16 : Please note that the reference (Lee et al. 2020) is not mentioned (cited) in the text. Add it to the text and link it to the reference or delete it from the reference list by making changes directly in the text or references.
Response: Resolved

AQ17 : Please note that the reference (Pruitt et al. 2015) is not mentioned (cited) in the text. Add it to the text and link it to the reference or delete it from the reference list by making changes directly in the text or references.
Response: Resolved

AQ18 : The caption for Figure 1 currently contains reference to colour used within the figure. For accessibility purposes reference to colour should be avoided unless essential to the understanding of the content. If the reference to colour is not essential to the understanding of the content please provide updated wording for the figure caption to remove reference to colour.
Response: The color reference is essential because the arrowheads identify different root developmental landmarks. This appl ies to Figures 1-10.

AQ19 : Please provide alt text for Figure 1, directly in the text. ‘Alt text’ is used by screen reading software to describe images to visually impaired readers. Guidance on creating alt text can be found at the following location: link. If you do not provide alt text we will use the following standard alt text: *For image description, please refer to the figure legend and surrounding text.*
Response: We agree with the standard alt text. This applies to Figure 1-10.

AQ20 : The caption for Figure 2 currently contains reference to colour used within the figure. For accessibility purposes reference to colour should be avoided unless essential to the understanding of the content. If the reference to colour is not essential to the understanding of the content please provide updated wording for the figure caption to remove reference to colour.
Response: Resolved

AQ21 : Please provide alt text for Figure 2, directly in the text. ‘Alt text’ is used by screen reading software to describe images to visually impaired readers. Guidance on creating alt text can be found at the following location: link. If you do not provide alt text we will use the following standard alt text: *For image description, please refer to the figure legend and surrounding text.*
Response: Resolved

AQ22 : The caption for Figure 3 currently contains reference to colour used within the figure. For accessibility purposes reference to colour should be avoided unless essential to the understanding of the content. If the reference to colour is not essential to the understanding of the content please provide updated wording for the figure caption to remove reference to colour.
Response: Resolved

AQ23 : Please provide alt text for Figure 3, directly in the text. ‘Alt text’ is used by screen reading software to describe images to visually impaired readers. Guidance on creating alt text can be found at the following location: link. If you do not provide alt text we will use the following standard alt text: *For image description, please refer to the figure legend and surrounding text.*
Response: Resolved

AQ24 : The caption for Figure 4 currently contains reference to colour used within the figure. For accessibility purposes reference to colour should be avoided unless essential to the understanding of the content. If the reference to colour is not essential to the understanding of the content please provide updated wording for the figure caption to remove reference to colour.

Response: Resolved

AQ25 : Please provide alt text for Figure 4, directly in the text. 'Alt text' is used by screen reading software to describe images to visually impaired readers. Guidance on creating alt text can be found at the following location: link. If you do not provide alt text we will use the following standard alt text: *For image description, please refer to the figure legend and surrounding text.*

Response: Resolved

AQ26 : The caption for Figure 5 currently contains reference to colour used within the figure. For accessibility purposes reference to colour should be avoided unless essential to the understanding of the content. If the reference to colour is not essential to the understanding of the content please provide updated wording for the figure caption to remove reference to colour.

Response: Resolved

AQ27 : Please provide alt text for Figure 5, directly in the text. 'Alt text' is used by screen reading software to describe images to visually impaired readers. Guidance on creating alt text can be found at the following location: link. If you do not provide alt text we will use the following standard alt text: *For image description, please refer to the figure legend and surrounding text.*

Response: Resolved

AQ28 : The caption for Figure 6 currently contains reference to colour used within the figure. For accessibility purposes reference to colour should be avoided unless essential to the understanding of the content. If the reference to colour is not essential to the understanding of the content please provide updated wording for the figure caption to remove reference to colour.

Response: Resolved

AQ29 : Please provide alt text for Figure 6, directly in the text. 'Alt text' is used by screen reading software to describe images to visually impaired readers. Guidance on creating alt text can be found at the following location: link. If you do not provide alt text we will use the following standard alt text: *For image description, please refer to the figure legend and surrounding text.*

Response: Resolved

AQ30 : The caption for Figure 7 currently contains reference to colour used within the figure. For accessibility purposes reference to colour should be avoided unless essential to the understanding of the content. If the reference to colour is not essential to the understanding of the content please provide updated wording for the figure caption to remove reference to colour.

Response: Resolved

AQ31 : Please provide alt text for Figure 7, directly in the text. 'Alt text' is used by screen reading software to describe images to visually impaired readers. Guidance on creating alt text can be found at the following location: link. If you do not provide alt text we will use the following standard alt text: *For image description, please refer to the figure legend and surrounding text.*

Response: Resolved

AQ32 : Please provide alt text for Figure 8, directly in the text. 'Alt text' is used by screen reading software to describe images to visually impaired readers. Guidance on creating alt text can be found at the following location: link. If you do not provide alt text we will use the following standard alt text: *For image description, please refer to the figure legend and surrounding text.*

Response: Resolved

AQ33 : The caption for Figure 8 currently contains reference to colour used within the figure. For accessibility purposes reference to colour should be avoided unless essential to the understanding of the content. If the reference to colour is not

essential to the understanding of the content please provide updated wording for the figure caption to remove reference to colour.

Response: Resolved

AQ34 : The caption for Figure 9 currently contains reference to colour used within the figure. For accessibility purposes reference to colour should be avoided unless essential to the understanding of the content. If the reference to colour is not essential to the understanding of the content please provide updated wording for the figure caption to remove reference to colour.

Response: Resolved

AQ35 : Please provide alt text for Figure 9, directly in the text. 'Alt text' is used by screen reading software to describe images to visually impaired readers. Guidance on creating alt text can be found at the following location: link. If you do not provide alt text we will use the following standard alt text: *For image description, please refer to the figure legend and surrounding text.*

Response: Resolved

AQ36 : The caption for Figure 10 currently contains reference to colour used within the figure. For accessibility purposes reference to colour should be avoided unless essential to the understanding of the content. If the reference to colour is not essential to the understanding of the content please provide updated wording for the figure caption to remove reference to colour.

Response: Resolved

AQ37 : Please provide alt text for Figure 10, directly in the text. 'Alt text' is used by screen reading software to describe images to visually impaired readers. Guidance on creating alt text can be found at the following location: link. If you do not provide alt text we will use the following standard alt text: *For image description, please refer to the figure legend and surrounding text.*

Response: Resolved

AQ38 : We have received files for publication as supplementary material.These will be published in the format provided, without edits. If any files need to be removed, specify by responding to this query, stating the filename. If any files need to be added, upload them directly or email them with your proof corrections. If any files need to be updated, upload them directly or email them, without altering the filename. We will seek editor approval for any changes to supplementary material which may delay publication of your article.

Response: Resolved

Tyrosine-sulfated peptide-induced flavonol biosynthesis controls elongation and differentiation in Arabidopsis primary root[AQ0]

Verso running head : *The Plant Cell*, 2026, Vol. XX, Issue XX

Recto running head : *The Plant Cell*, 2026, Vol. XX, Issue XX

Maria Florencia Ercoli[1,2,3], Alexandra M. Shigenaga[1,2], Artur Teixeira de Araujo Jr[1,2,4], Katherine B. Louie[5,6], Benjamin P. Bowen[5,6], Tracy S. Weitz[1,2], Sangeetha Ramesh[1,2], Rashmi Jain[1,2], Trent R. Northen[5,6], Pamela C. Ronald[1,2,3,4,*][AQ1][AQ2]

1 Department of Plant Pathology, University of California, Davis, CA 95616, USA[AQ3]

2 The Genome Center, University of California, Davis, CA 95616, USA[AQ4]

3 The Innovative Genomics Institute, University of California, Berkeley, CA 94720, USA[AQ5]

4 DOE ~~The~~ Joint BioEenergy Institute, Emeryville, CA 94608, USA[AQ6]

5 Environmental Genomics and Systems Biology Division, Lawrence Berkeley National Laboratory, Berkeley, CA 94720,

USA[AQ7]

6 Joint Genome Institute, Lawrence Berkeley National Laboratory, Berkeley, CA 94720, USA[AQ8]

* Corresponding author: Email: pcronald@ucdavis.edu[AQ9] Department of Plant Pathology, University of California, Davis, 1 Shields Drive, Davis, CA 95616, USA, pcronald@ucdavis.edu

Author Note

The author responsible for distribution of materials integral to the findings presented in this article in accordance with the policy described in the Instructions for Authors (https://academic.oup.com/plcell/pages/General-Instructions) is: Pamela C. Ronald (pcronald@ucdavis.edu)

Supplementary Material

koag180_Supplementary_Data

HISTORY: received: 2025-04-29 **accepted**: 2026-03-07

Abstract

In Arabidopsis (*Arabidopsis thaliana*) roots, growth initiation and cessation are organized into distinct zones. How regulatory mechanisms are integrated to coordinate these processes and maintain proper growth progression over time remains poorly understood. Here, we demonstrate that the peptide hormone PLANT PEPTIDE CONTAINING SULFATED TYROSINE 1 (PSY1) promotes root growth by controlling cell elongation. Higher levels of PSY1 lead to longer differentiated cells with a shootward displacement of characteristics common to mature cells. PSY1 activates genes involved in the biosynthesis of flavonols, a group of plant-specific specialized metabolites. Consistent with these transcriptional changes, metabolomic analysis reveals an enrichment of diverse flavonol glycosides upon PSY1 treatment. Using genetic and chemical approaches, we show that PSY1-mediated flavonol accumulation is localized to the differentiation zone and is required for PSY1 function. PSY1 signaling in this zone is associated with a reduction of hydrogen peroxide accumulation and a decrease in auxin-induced gene expression. These findings support a model where PSY1 signals the developmental-specific accumulation of specialized metabolites to regulate the extent of cell elongation and progression to maturation.

One-sentence summary

A plant peptide hormone promotes root growth in Arabidopsis by triggering the accumulation of specialized metabolites that regulate cell elongation and progression to maturation.

Introduction

In multicellular organisms, growth involves cell proliferation and expansion. The shape and final dimensions of an organ are determined by the balance between growth initiation and cessation. In roots, these dynamics underlie primary growth, causing the root to extend along its longitudinal axis (Svolacchia et al. 2020). Although it is known that the establishment and maintenance of developmental boundaries are critical for the spatiotemporal regulation of growth initiation and cessation (Žádníková and Simon 2014), how different regulatory networks are integrated to control the magnitude of cellular growth in roots is not well understood.

In the *Arabidopsis thaliana* primary root, cellular growth is initiated, maintained, and eventually terminated (Fig. 1a[AQ10], left side of the panel; Ivanov and Dubrovsky 2013). The different cell types that constitute the root arise from generative cell divisions of stem cells located in the stem cell niche (SCN) located at the proximal (rootward) end of the root tip. The SCN is maintained by a small group of slowly dividing organizer cells known as the quiescent center (QC) (Heyman et al. 2014). More distally (shootward) from the QC, in the meristematic zone (MZ), proliferating cells provide the necessary number of cells for organ growth (Ivanov and Dubrovsky 2013). Cells stop dividing at the transition zone (TZ) but continue to grow rapidly by directional expansion in the adjacent elongation zone (EZ) (

Beemster and Baskin 1998; Di Mambro et al. 2017; Salvi et al. 2020a). Cell elongation slows down in the distal parts of the EZ in what is defined as the start of growth cessation (Liu et al. 2022). Finally, growth ceases in the differentiation zone (DZ), and cells mature into their final shape and function (Cajero Sánchez et al. 2018). Because postembryonic root growth is indeterminate, these processes are continual, resulting in a developmental gradient along the root longitudinal axis, referred to as root zonation (Fig. 1a, left side of the panel; Scheres et al. 2002).

Figure 1

Loss of PSY1 impairs Arabidopsis root growth. a) A scheme describing *A. thaliana* root zonation (left side of the panel). SCN, stem cell niche; MZ, meristematic zone; EZ, elongation zone; DZ, differentiation zone. A 7-d-old Arabidopsis primary root expressing a *PSY1* promoter-GFP transcriptional reporter (*ProPSY1:GFP*) (green) (right side of the panel). Cell walls were stained with PI (magenta). b) Root growth, (c) root elongation rate (mm/h) ($n = 47$ seedlings), and (d) cortical cell length profile ($n = 12$ seedlings) in wt and *psy1* seedlings grown for 6 d on 1×MS vertical plates with or without 50 nM of synthetic PSY1. The MZ size (e and f, $n = 12$ seedlings) and mature cortical cell length (g and h, $n = 100$ cells) are highlighted. The limits of a representative MZ (e) and mature cortical cells (g) are shaded in pale orange and green, respectively. i) Distance from QC to the first root hair bulge at stage +2 (RHB 2+) ($n = 23$ seedlings), (j) root tip architecture, (k) length between consecutive root hairs in 1 trichoblast file ($n = 78$), (l and m, $n = 12$ seedlings) distance from end of MZ (l) and from QC (m) to differentiated vascular elements (Diff. protoxylem) revealed by basic fuchsin staining from *wt* and *psy1* seedlings grown for 6 d on 1×MS vertical plates with or without 50 nM of synthetic PSY1. In (j), the length between consecutive root hairs in 1 trichoblast file is highlighted in magenta. In (l), the gray squares indicate the zone where the deposition of lignin starts in the protoxylem, as revealed with basic fuchsin staining, and organ boundaries are marked by white dashed lines. In (c), (f), (h), (i), (k), and (m), the data shown are box and whisker plots combined with scatter plots; each dot indicates the measurement of the designated parameter listed on the *y*-axis. The box spans the interquartile range (25th to 75th percentiles), the center line denotes the median, and whiskers extend to the smallest and largest observed values. Different letters indicate significant differences, as determined by 1-way ANOVA followed by Tukey's multiple comparison test ($P < 0.05$). The purple arrowheads mark the position of the QC, the pale orange arrowheads mark the end of the meristem, where cells start to elongate, the green arrowheads indicate the mature cortical cell size, and the magenta arrowhead points to the first root hair bulge, defined as stage +2, indicating the end of the elongation zone in the epidermis. For presentation purposes, images in (a), (j), and (l) were placed on a uniform background to standardize panel shape. Individual tiles were acquired and then combined using the LSCM merging function to generate the final complete root images in (a) and (l).[AQ18][AQ19]

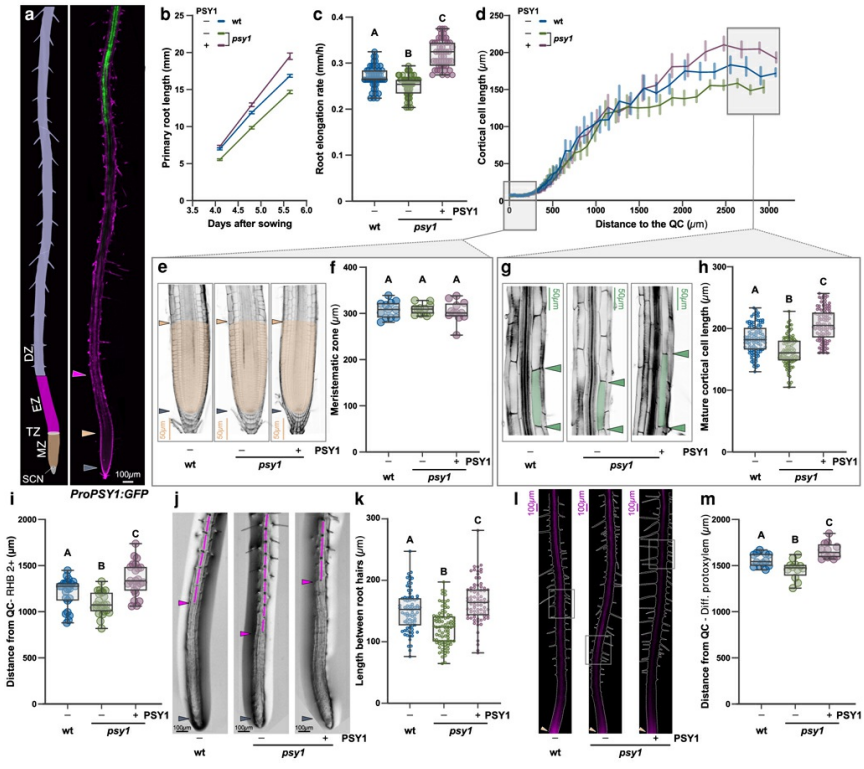

To ensure proper root zonation, a combination of mechanical forces, transcriptional regulators, phytohormones, and metabolic inputs interact to establish the developmental boundaries that maintain the balance between growth initiation and cessation (Zluhan-Martínez et al. 2021). The transition between the MZ and EZ involves a complex interplay of phytohormones, primarily auxin

and cytokinin (Salvi et al. 2020a). Polar auxin transport (PAT) generates a gradient in the root with a maximum at the SCN. This gradient regulates the distribution of *PLETHORA* (*PLT*) transcription factors (Blilou et al. 2005; Salvi et al. 2020b). PLT proteins also display a graded distribution and modulate root zonation in a dosage-dependent manner: high levels are required for maintenance of the SCN, intermediate levels induce rapid cell divisions in the MZ, and low levels facilitate cell elongation and differentiation (Aida et al. 2004; Galinha et al. 2007; Mähönen et al. 2014). Cytokinin controls PAT and auxin degradation, generating an auxin minimum precisely positioning the TZ (Di Mambro et al. 2017). In the elongation/differentiation transition, distinct mature cellular characteristics such as cell wall structure (Somssich et al. 2016), microtubule orientation (Montesinos et al. 2020), root hair development in the epidermis (Denninger et al. 2019), and lignified secondary cell walls in the protoxylem (Růžička et al. 2015), among others, point to a pronounced shift in cell identity and function across these root regions. The interplay between regulatory mechanisms underpinning this second developmental boundary where the cessation of rapid cell elongation and maturation of root cells occurs remains underexplored.

Alongside classic plant hormones, small tyrosine-sulfated peptides play significant roles in the complex regulatory networks controlling root growth and are thus candidates for signaling in the developmental trajectories in root zonation (Matsubayashi 2014; Kaufmann and Sauter 2019). Functioning as extracellular signals, these peptide hormones synchronize cellular activities across tissues. Typically, they bind to leucine-rich repeat receptor-like kinases (LRR-RLKs) to trigger specific signaling pathways (Ercoli et al. 2022). Sulfation of a tyrosine residue in the peptide sequence, a posttranslational modification carried out by *TYROSYLPROTEIN SULFOTRANSFERASE* (*TPST*), is required for signaling activity, as it regulates peptide affinity for its cognate receptor (Komori et al. 2009; Wang et al. 2015; Song et al. 2016; Stewart and Ronald 2022). Among the best-characterized examples are the ROOT MERISTEM GROWTH FACTOR (RGF) peptides, a family of functionally redundant signaling molecules, including RGF1, known to control meristem size (Matsuzaki et al. 2010). RGF1 signaling regulates the spatial distribution and expression levels of PLT transcription factors to sustain stem cell identity and promote cell proliferation (Matsuzaki et al. 2010; Ou et al. 2016; Shinohara et al. 2016). Subsequent studies showed that this regulation depends on RGF1-mediated modulation of reactive oxygen species (ROS) gradients, which influence the oxidative environment of the meristem and enhance PLT2 protein stability to maintain meristem size (Yamada et al. 2020). The exogenous application of RGF1 alone is not sufficient to fully complement the *tpst-1* mutant phenotype; however, the addition of 2 other tyrosine-sulfated peptides, PHYTOSULFOKINE (PSK) and PLANT PEPTIDE CONTAINING SULFATED TYROSINE 1 (PSY1), restores root growth in *tpst-1* to wild-type (wt) levels (Komori et al. 2009; Matsuzaki et al. 2010), underscoring the complementary roles of these peptide hormones in root development. The *PSY* family in Arabidopsis is composed of 9 members (Amano et al. 2007; Ogawa-Ohnishi et al. 2022). To exert their function, these peptides bind to 3 cognate LRR-RLKs known as *PSYR* or *ROOT ELONGATION RECEPTOR KINASES (REKs)1/2/3* (Ogawa-Ohnishi et al. 2022; Wang et al. 2022). The triple PSYR knockout (*psyr123* or *tri-1*) displays an elongated root phenotype compared with wt plants, suggesting that PSYR1/2/3 signaling negatively regulates root growth (Ogawa-Ohnishi et al. 2022; Wang et al. 2022). The application of synthetic PSY peptides enhances root growth of wt and *tpst* knockout plants but not the triple receptor mutant, supporting a role for PSYR1/2/3 as receptors for PSY peptides (Amano et al. 2007; Pruitt et al. 2017; Ogawa-Ohnishi et al. 2022). Among this peptide family, PSY1 is the most extensively studied, particularly its association with the regulation of mature cell size in the root cortex and seedling cuticle development (Amano et al. 2007; De Giorgi et al. 2021). Despite these advances, the broader contribution of PSY signaling in plant root growth remains to be fully characterized.

Another layer of signaling that controls root development involves plant-specialized metabolites, including flavonols, a type of flavonoid (Daryanavard et al. 2023). In Arabidopsis, the central flavonoid biosynthetic pathway is well characterized and produces 3 main aglycone scaffolds, kaempferol, quercetin, and isorhamnetin (Saito et al. 2013). These aglycones then undergo extensive tailoring modifications, including hydroxylation, methylation, and glycosylation, which generate the wide diversity of flavonols detected in roots (Saito et al. 2013). The developmental roles of flavonols are best characterized using mutants that accumulate varying levels of these metabolites. The genetic and biochemical diversity of *transparent testa (tt)* mutants has been instrumental in dissecting flavonoid functions (Koornneef 1990). The use of the *tt4* allelic series of the *CHALCONE SYNTHASE* (*CHS*) locus, which encodes the first enzyme in the flavonoid biosynthetic pathway, has provided a framework for understanding how differences in enzyme activity translate into variation in flavonol accumulation and developmental outcomes (Saslowsky et al. 2000). PAT from the shoot toward the root tip is elevated in *tt4* mutants, consistent with evidence showing that flavonols function as negative regulators of auxin transport (Brown et al. 2001; Peer et al. 2004; Lewis et al. 2011). Moreover, flavonols have been shown to stabilize PIN efflux carrier complexes, mimicking the effect of the auxin transport inhibitor 1-naphthylphthalamic acid, thereby restricting auxin flow (Teale et al. 2021). In addition, *tt4* mutants display elevated ROS levels in root hairs, consistent with the well-established antioxidant activity of flavonoids (Agati et al. 2012; Gayomba and Muday 2020). The appearance of root hairs closer to the tip in *tt4* mutants is accompanied by an increased number of root hairs due to a higher frequency of trichoblast cells in the epidermis (Gayomba and Muday 2020). Furthermore, because ROS balance can modify auxin distribution (Pasternak et al. 2023), a complex interplay between flavonols, ROS, and auxin transport is involved in the regulation of root development.

In this study, we demonstrate that PSY1 regulates root growth by controlling the magnitude that cells elongate before achieving their final, differentiated size. Integrated transcriptomic and metabolomic profiling of PSY1-treated roots revealed a concerted induction of flavonol biosynthetic genes and an enrichment of flavonol glycosides. Loss-of-function mutants and chemical treatments indicate that flavonol biosynthesis is required for PSY1-induced root growth. Consistent with known flavonol functions, PSY1 signaling is associated with a reduction of hydrogen peroxide accumulation and a decrease in auxin-induced gene expression. These findings indicate that root zonation requires spatial regulation of flavonol accumulation, significantly advancing our understanding of the mechanisms that regulate cell elongation and differentiation in Arabidopsis roots.

Results

PSY1 controls cell elongation and differentiation in primary roots

To explore the role of PSY1 in Arabidopsis (*A. thaliana*) primary root growth, we examined *PSY1* promoter expression in Arabidopsis roots. We found that *PSY1* is highly expressed in the DZ as determined using publicly available gene expression profiles of manually dissected root tissue segments corresponding to MZ, EZ, and DZ (Brady et al. 2007; Fig. S1a). A matching expression profile was obtained when utilizing the single-cell Arabidopsis root atlas (Shahan et al. 2022; Fig. S1b). To validate these results, we generated 10 independent transgenic lines expressing the transcriptional reporter *ProPSY1:GFP* (*PSY1* promoter-driven GFP) in the wt Col-0 background. We observed that PSY1 promoter activity gradually increased in the progression of the DZ, with the GFP signal starting to rise ~2,000 μm from the QC (Figs. 1a and S1c). Interestingly, when we analyzed *ProPSY1:GFP* expression in the DZ, we found that the GFP signal was almost undetectable in the epidermis, consistent with the pattern of *PSY1* expression in various root tissues at different developmental stages, as documented in the single-cell Arabidopsis root atlas (Shahan et al. 2022; Fig.S1, b and d). Although *PSY1* is not expressed in the epidermis, the PSYR receptors, with the exception of PSYR1, are expressed more broadly in roots, including both trichoblast and atrichoblast cells of the elongation and maturation zones (Fig. S2).

To investigate the function of PSY1 in root development, we generated ectopic expression lines in a wt background using the constitutive 35S promoter (*Pro35S:PSY1*). We validated PSY1 accumulation using high-resolution mass spectrometry and quantitative reverse transcription polymerase chain reaction (RT-qPCR) (Figs. S3 and S4a). Consistent with previous reports, these plants developed longer primary roots (Fig. S4, b and c; Amano et al. 2007). The same phenotype was observed when wt plants were treated with synthetic PSY1 (Fig. S5, a to c). Exogenous application of PSY1 also partially restored root growth in the tyrosylprotein sulfotransferase mutant, *tpst-1*, which is deficient in biosynthesis of all tyrosine sulfated peptides (Fig. S5, a to c; Komori et al. 2009; Matsuzaki et al. 2010). Synthetic PSY1 treatment did not affect the longer root phenotype observed in the *psyr1,2,3* triple receptor mutant (Fig. S6, a and b; Ogawa-Ohnishi et al. 2022; Wang et al. 2022), which supports the known role for *PSYR1/2/3* as receptors for PSY peptides. Finally, the *psy1* knockout (De Giorgi et al. 2021) displayed reduced root length and elongation rates (Fig. 1, b and c). Synthetic PSY1 treatment rescued the root growth defect in the *psy1*, resulting in a phenotype resembling that of wt roots subject to PSY1 treatment (Figs. 1, b and c and S5, a to c).

To further examine the root growth phenotype, we constructed a cell length profile by measuring the length of individual cortical cells from the QC to the DZ. In a typical cell length profile, cell length remains relatively short and constant in the MZ, sharply increases in the EZ, and eventually levels off in the DZ, where cells attain their final size and identity (Ivanov and Dubrovsky 2013). Our profile analysis revealed that the MZ length in *psy1*, *Pro35S:PSY1*, and *psyr1,2,3* are indistinguishable from wt plants (Figs. 1, d to f, S4, d to f and S6, c to e). Additionally, the short MZ in *tpst-1* mutants remained unaffected when grown in media supplemented with synthetic PSY1 (Fig. S5, d to f). Consistent with these findings, the expression and distribution of the G2-to-mitosis transition marker *CYCLINB1;1*, commonly used to assess cell proliferation in the MZ (Ivanov and Dubrovsky 2013), were unchanged in the plants expressing ectopic PSY1 (Fig. S7, a to d). These results indicate that PSY1 does not regulate cell proliferation in the MZ.

Because the establishment of the TZ relies on the auxin/*PLETHORA*/cytokinin regulatory node (Galinha et al. 2007; Di Mambro et al. 2017; Salvi et al. 2020a), we investigated the responses of this molecular network following synthetic PSY1 treatment. We observed no significant differences in the intensity and distribution of auxin-induced gene expression and cytokinin response reporter lines (*DR5v2:n3GFP* [Liao et al. 2015] and *pTCSn::GFP* [Liu and Müller 2017], respectively) compared with untreated plants (Fig. S7, e to h). Additionally, there were no differences in localization and expression of *PLETHORA1* (*PLT1*) between PSY1-treated and untreated plants based on our analysis of a transcriptional reporter line (*ProPLT1:CFP*) (Fig. S7, i to k). Because *PLT1* expression is also controlled post-translationally (Matsuzaki et al. 2010; Yamada et al. 2020), we evaluated the response of a plant expressing translational fusion (*ProPLT1-PLT1:YFP*). *ProPLT1-PLT1:YFP* expression did not change in response to PSY1 treatment (Fig. S7, l to n). In contrast, when treated with ROOT MERISTEM GROWTH FACTOR 1 (RGF1), a small tyrosine-sulfated peptide known to regulate MZ size by stabilizing PLT proteins, the PLT1-YFP signal showed an enhanced and broader expression in the MZ. Together, these results show that PSY1 does not modify the position of the TZ and, therefore, does not affect the size of the MZ.

Next, we leveraged the cell length profiles to investigate the role of PSY1 in the control of cell elongation. We found that where the cortical cells in the *psy1* mutant reached their final cell size, cortical cells were still elongating in the wt plant, suggesting a premature exit from elongation in the mutant (Fig. 1d). Consistent with this, *psy1* mutants exhibited significantly shorter mature cortical cells compared with wt (Fig. 1, d, g, and h). Conversely, when *psy1* mutants were grown in media supplemented with synthetic PSY1, the cortical cells continued to elongate, whereas cells in the wt stalled, resulting in significantly longer mature cortical cell sizes compared with those of wt plants (Fig. 1, d, g, and h). Similar effects were observed in *tpst-1* plants grown in media supplemented with PSY1, as well as in wt plants expressing *Pro35S:PSY1* and in the triple receptor mutant *psyr1,2,3* (Figs. S4, d, g, h, S5, d, g, h and S6, c, f, g). These findings denote a role for PSY1 primarily controlling root growth by defining the extent to which cells elongate before cells reach their final, differentiated size.

If our hypothesis is correct, PSY1 may also affect the distance from the QC at which cell elongation slows down in other tissues. In the trichoblast cell files of the epidermis, the onset of root hair development marks the cessation of rapid cell elongation, followed by minimal further cell elongation as these cells attain their mature size (Le et al. 2004). To explore this in the context of PSY1 signaling, we measured the distance from the root tip to where the first root hair bulge at stage +2 can be identified (Denninger et al. 2019). Notably, in *psy1* mutants, we observed that this distance is reduced compared with wt plants (Fig. 1, i and j). In line with a premature appearance of root hairs and exit of cell elongation, the length between consecutive root hairs in 1 trichoblast file was reduced in *psy1* (Fig. 1, j and k). Additionally, secondary cell wall formation, as evidenced by the characteristic helical lignin pattern, a maturation cue in the tracheary elements of protoxylem (PX) (Li et al. 2022), appeared closer to the root tip of *psy1* plants as visualized using basic fuchsin staining (Fig. 1, l and m). These findings suggested that in *psy1* mutants, hallmarks of maturation in different tissues have shifted toward the root tip. In contrast, growing *psy1* mutants in media supplemented with synthetic PSY1 led to root hair initiation farther from the root tip, increased distance between root hairs in a single trichoblast cell file, and shootward displacement of lignin deposition in PX (Fig. 1, i to m). Similar effects were observed in *tpst-1* plants grown in media supplemented with PSY1, as well as in wt plants expressing *Pro35S:PSY1* and in the triple receptor mutant *psyr1,2,3* (Figs. S4, i to m, S5, i to m, and S6, h to l). Altogether, these results indicate that PSY1 functions as a crucial signal necessary for a normal root zonation.

PSY1 regulates genes highly expressed in elongation and DZs

To investigate how PSY1 controls root zonation, we carried out RNA-sequencing (RNA-seq) profiling of roots treated with synthetic PSY1. For these experiments, we harvested the root tips, including the DZ, from 5-d-old wt seedlings treated with PSY1 for 4 h (Fig. 2a). Because seedlings need to be treated with synthetic PSY1 for at least 24 h to exhibit root zonation changes (Fig. S8, a and b), this suggests that the changes observed in RNA level modifications in this experiment are unlikely to result from anatomical alterations. The RNA-seq analysis revealed that 253 genes (92 increased and 161 decreased transcriptional abundance) were differentially expressed after 4 h of PSY1 treatment (Data Set S1).

Figure 2

PSY1 regulates genes highly expressed in the elongation and DZs. a) Seedlings were grown on a permeable mesh placed on a clear agar substrate. After 5-d, seedlings were transferred to a control medium or medium containing PSY1 (50 nM) by moving the mesh to the selected media. After 4 h, samples were harvested. RNA was extracted from designated root zones. b) Scheme of a root showing developmental zones. Horizontal lines define the sections (L1–L12) of the longitudinal Root Gene Expression Atlas (Brady et al. 2007). Col, Columella. Sections 1 to 6 comprise the MZ; 7 and 8, the Elongation zone (EZ); and 9 to 12, the DZ. Expression along the root's longitudinal axis of genes activated (c) or repressed (d) after PSY1 treatment. *Z*-scores were calculated across samples and expressed as a heat map. The double red line separates genes preferentially expressed in columella and meristematic regions (left) from those that present a maximum expression in the elongation and DZ (right). e) Bubble plot for KEGG pathway enrichment analysis of genes activated or repressed after PSY1 treatment (Data Set S3). The *y*-axis shows the FDR in a negative Log_{10} scale, whereas the *x*-axis is fixed, and terms from the same KEGG subtree are located closer to each other. The size of each circle represents the term Fold Enrichment in the Log_{10} scale.**[AQ20][AQ21]**

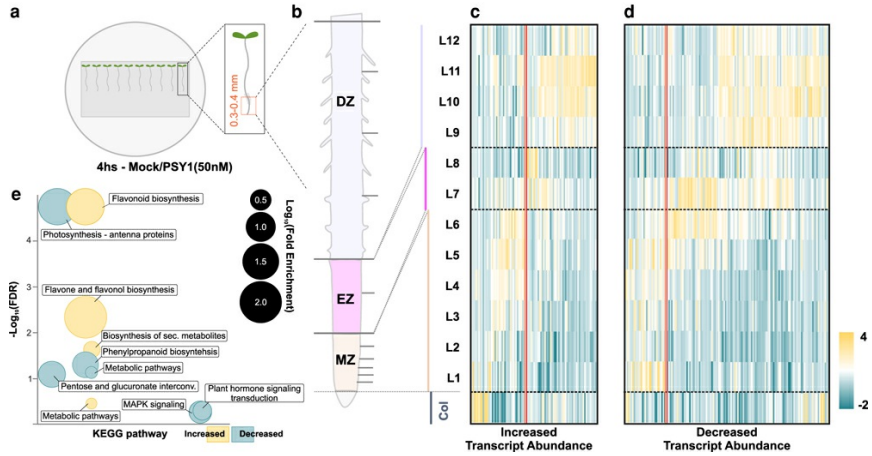

Given the role of PSY1 controlling growth by determining the magnitude of cell elongation and mature cell size without affecting cell proliferation, we anticipated that genes downstream of PSY1 signaling would primarily be expressed outside the MZ. To test this hypothesis, the expression patterns of the PSY1-responsive genes were analyzed in the developmental stage-specific gene expression database (Brady et al. 2007; Fig. 2, b to d). We found that 57% of the genes with increased transcript abundance following PSY1 treatment (51 out of 89 genes) (Fig. 2c) and 80% of the genes with decreased transcript abundance (117 of 146 genes) (Fig. 2d) exhibited a peak of expression in a region corresponding to the EZ and DZ. This spatial pattern shows that PSY1 controls genes preferentially expressed in the same zones of the root where the PSY1-associated phenotypes are observed.

Gene Ontology (GO) and Kyoto Encyclopedia of Genes and Genomes (KEGG) pathway enrichment analyses were conducted to explore the functions of PSY1-responsive genes (Figs. 2e, S8, c and d and Data Sets S2 and S3). Notably, secondary metabolic processes and flavonol biosynthetic pathways were significantly enriched categories among the genes with increased transcript abundance following PSY1 treatment (Figs. 2e, S8c and Data Sets S2 and S3). Flavonols, a class of flavonoids that are specialized metabolites in plants, include compounds such as quercetin and kaempferol, along with their glycosylated derivatives, which are commonly found in Arabidopsis roots (Saito et al. 2013). Enzymes responsible for synthesizing these 2 specific flavonol scaffolds were upregulated in response to PSY1 treatment (Fig. 3, a and b and Data Set S1). Additionally, the transcription factor *MYB12*, which is known to control flavonol biosynthesis primarily in the root (Mehrtens et al. 2005; Stracke et al. 2007), the multidrug and toxin efflux flavonoid transporter *DTX35* (Thompson et al. 2010), the *RHAMNOSE SYNTHASE RHM1/ROL1* (Ringli et al. 2008), and the *3-KETOACYL-COA THIOLASE* isoform *KAT5* (Perez de Souza et al. 2020) were also upregulated by PSY1 treatment (Fig. 3, a and b and Data Set S1). *KAT5* and *RHM1* were previously shown to be closely associated with genes involved in flavonoid biosynthesis in a co-expression analysis (Yonekura-Sakakibara et al. 2008). Furthermore, our time course study of whole seedlings treated with synthetic PSY1 coupled with RT-qPCR demonstrated that a subset of genes differentially regulated after 4 h of PSY1 treatment maintained their expression levels at 8, 12, and 48 h (Fig. S8g).

Figure 3

PSY1 regulates genes that code for enzymes involved in the production of flavonols. a) Flavonoid biosynthetic pathway. Circles represent the flavonoid biosynthesis enzymes. The metabolites are labeled with rectangular boxes. Yellow circles are the genes coding for enzymes activated after PSY1 treatment, with circle size proportional to the fold-change (FC) in transcript abundance. Yellow circles with red borders denote the genes coding for enzymes that are also positively regulated by MYB12, according to (Stracke et al. 2007). b) Summary table of differentially expressed genes following PSY1 treatment, including Locus ID, FC, FDR, and gene names (Data Set S1). FC values represent transcript abundance in PSY1-treated roots relative to untreated control roots. Genes that are part of the pathway but not regulated by PSY1 include: *C4H*, cinnamic acid 4-hydroxylase; *ACC*, acetyl-CoA carboxylase; *OMT1*, o-methyltransferase 1; *DFR*, dihydroflavonol 4-reductase; *ANS*, anthocyanidin synthase; *ANR*, anthocyanidin reductase; *F3ARAT*, flavonol 3-o-arabinosyltransferase; *F7GlcT*, flavonol 7-o-glucosyltransferase; *F7RhaT*, flavonol 7-o-rhamnosyltransferase. Names of the mutant lines of genes coding for enzymes used in subsequent experiments are in parentheses (Table S1).**[AQ22][AQ23]**

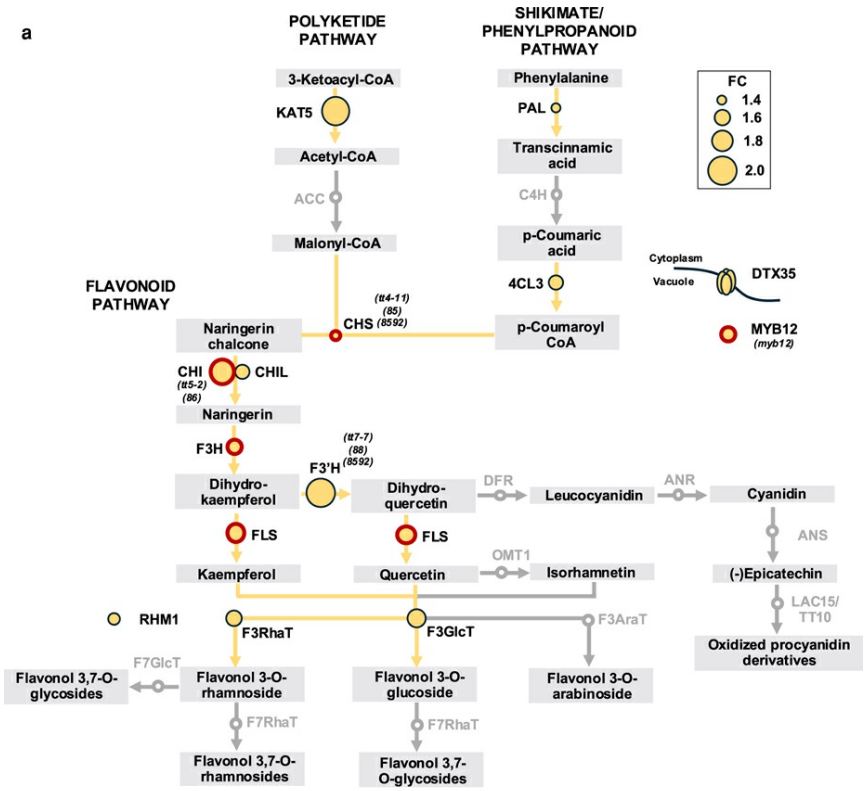

ID	logFC	FDR	FC		Name
AT5G07990	1.01	2.90E-22	2.01	F3'H	FLAVONOID 3-HYDROXYLASE
AT5G48880	1.00	4.90E-17	2.00	*KAT5*	3-KETOACYL-COA THIOLASE
AT3G55120	0.93	1.37E-14	1.90	CHI	CHALCONE ISOMERASE
AT1G30530	0.78	1.07E-03	1.72	*F3RHAT*	UDP-GLUCOSYL TRANSFERASE 78D1
AT4G25640	0.74	1.99E-09	1.67	*DTX35*	DETOXIFYING EFFLUX CARRIER 35
AT5G08640	0.69	5.19E-09	1.61	FLS1	FLAVONOL SYNTHASE
AT1G65060	0.68	4.07E-08	1.60	4CL3	4-COUMARATE:COA LIGASE 3
AT3G51240	0.62	7.48E-13	1.53	*F3H*	FLAVANONE 3-HYDROXYLASE
AT5G17050	0.57	3.14E-09	1.48	*F3GLCT*	UDP-GLUCOSYL TRANSFERASE 78D2
AT2G47460	0.53	4.72E-03	1.45	*MYB12*	*R2R3-MYB*
AT5G05270	0.52	1.34E-09	1.43	CHIL	CHALCONE-FLAVANONE ISOMERASE FAMILY PROTEIN
AT5G13930	0.47	4.88E-08	1.38	CHS	CHALCONE AND STILBENE SYNTHASE
AT2G37040	0.34	4.90E-02	1.27	PAL1	PHENYLALANINE AMMONIA-LYASE 1
AT1G78570	0.31	1.71E-03	1.24	*RHM1*	UDP-RHAMNOSE SYNTHASE 1

Recent research has suggested that PSY-family peptides play a role in repressing PSYR function, thereby facilitating growth (Ogawa-Ohnishi et al. 2022). To further explore this hypothesis, we investigated whether synthetic PSY1 treatment could mimic the effects of PSYR loss at the molecular level. We conducted KEGG pathway enrichment analysis using the 1,947 genes with increased transcript abundance in the triple PSYRs mutant background (*psyr1,2,3* or *tri-1*), as reported by (Wang et al. 2022). Notably, categories related to flavonoid and phenylpropanoid biosynthesis were significantly enriched (Fig. S8e and Data Set S4). Additionally, among the 41 genes with increased transcript abundance following both PSY1 treatment and the triple PSYR mutant, 13 were associated with flavonol biosynthesis (Fig. S8f). Collectively, these findings indicate that synthetic PSY1 treatment and PSYR loss both increase the expression of genes involved in the biosynthesis of specialized metabolite intermediates.

PSY1 regulates flavonol accumulation in the DZ

Previous studies have revealed that flavonoid accumulation is developmentally regulated and occurs in a tissue-specific manner, matching the expression pattern of genes involved in early flavonoid biosynthesis (Jackson et al. 1992; Peer et al. 2001). Using publicly available transcriptomics data sets of manually dissected root tissue segments corresponding to MZ, EZ, and DZ (Brady et al. 2007), we found that the expression of genes that produce the majority of flavonols, including *CHALCONE SYNTHASE* (*CHS*), *CHALCONE ISOMERASE* (*CHI*) , *CHALCONE ISOMERASE*-LIKE (*CHIL*) , *FLAVANONE 3-HYDROXYLASE* (*F3H*) , *FLAVONOID 3-HYDROXYLASE* (*F3′H*), and *FLAVONOL SYNTHASE 1* (*FLS1*) exhibit similar expression patterns in the root, with peaks of expression at the end of the MZ and in the DZ (Fig. S9a). Consistent with this, *MYB12,* which regulates the expression of these genes (Stracke et al. 2007; Fig. 3), reaches its maximum expression level in the DZ (Fig. S9a). Also, as previously described in the analysis of the tissue-specific localization of these proteins (Gayomba and Muday 2020), these genes appeared highly expressed in ground tissue and stele, but they were barely detected in the epidermis (Fig. S9b; Shahan et al. 2022).

Because PSY1 phenotypes were observed in the EZ and DZ, we hypothesized that PSY1 may specifically regulate the biosynthesis of these specialized metabolites in these developmental zones. To test this, we analyzed *ProCHS:CHS-GFP* and *ProFLS1:FLS1-GFP* reporter lines (Fig. 4, a and f). These lines express *CHS* and *FLS1* fused to GFP under the control of their native promoters. We found

that synthetic PSY1 treatment increased GFP expression of both *ProCHS:CHS-GFP* and *ProFLS1:FLS1-GFP* in the DZ (Fig. 4, b, c, g and h). No significant changes were observed at the end of the MZ or the onset of root hair development (Fig. 4, d, e, i and j).

Figure 4

PSY1 promotes *CHS* and *FLS1* expression in the DZ. Expression of GFP reporter lines of *CHS* (*ProCHS:CHS-GFP*) (a to e) and *FLS1* (*ProFLS1:FLS1-GFP)* (f—to j). The images in (a) and (f) show GFP fluorescence in green and cell walls stained with PI in magenta in the middle focal plane. In the regions marked by rectangles, *ProCHS:CHS-GFP* (b to e) and *ProFLS1:FLS1-GFP* (g to j) GFP intensity was quantified in 6-d-old seedlings transferred to 1×MS vertical plates with or without 100 nM of synthetic PSY1 for 6 h. Sum projections generated from 30 z-section images for each region were used for this quantification. In (c) and (h), are representative maximum projections of the DZ to illustrate increased *CHS* and *FLS1* signal following PSY1 treatment. GFP fluorescence intensity profile is shown using RGB-rainbow false color with its color scale bar; white dashed lines mark organ boundaries. In (b), (d), (e), (g), (i), and (j), the fluorescence intensity is plotted as a fold change relative to the control. The data shown are box and whisker plots combined with scatter plots; each dot represents an independent seedling measurement. The box spans the interquartile range (25th to 75th percentiles), the center line denotes the median, and whiskers extend to the smallest and largest observed values. Representative images of 2 independent experiments ($n = 10$ to 12 seedlings/experiment) are shown. In (b), (d), (e), (g), and (i) *P*-values are calculated by a 2-tailed Student's *t*-test. In (j), *P*-values were calculated using a 2-tailed Welch's *t*-test The purple arrowheads mark the position of the QC, the pale orange arrowheads mark the end of the meristem, where cells start to elongate, and the magenta arrowhead points to the first root hair bulge, defined as stage +2, indicating the end of the elongation zone in the epidermis. For presentation purposes, images in (a) and (f) were placed on a uniform background to standardize panel shape. Individual tiles were acquired and then combined using the LSCM merging function to generate the final complete root images in (a) and (f).**[AQ24][AQ25]**

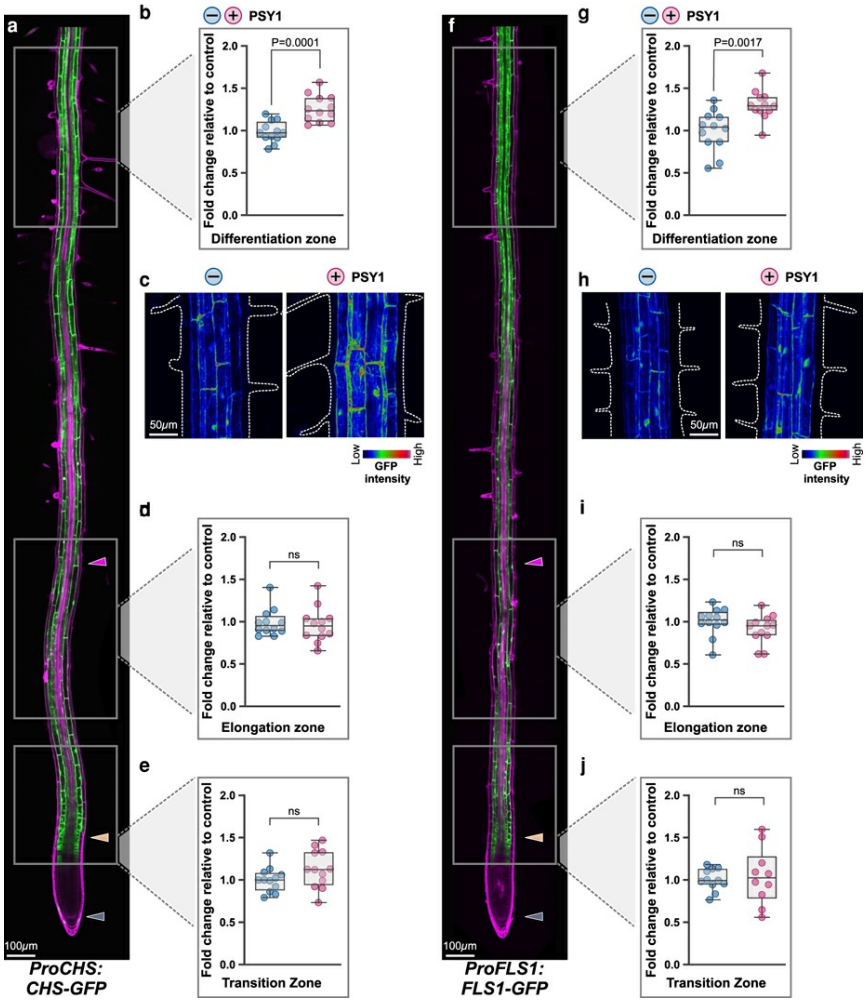

We next investigated whether *CHS* and *FLS1* expression patterns correlate with metabolite accumulation. For these experiments, we utilized the flavonol-specific dye diphenylboric acid 2-aminoethyl ester (DPBA). Kaempferol-DPBA (K-DPBA) and quercetin-DPBA (Q-DPBA) exhibit distinct spectral properties, enabling independent quantification of these 2 flavonols (Lewis et al. 2011). Consistent

with the localization of flavonol biosynthetic enzymes, K-DPBA and Q-DPBA signals were detected both at the end of MZ and in the DZ (Fig. 5a), with fluorescence peaking 300 μm from the root tip (Gayomba and Muday 2020). To visualize and quantify DPBA fluorescent signals along the root longitudinal axis, we generated plot profiles for K-DPBA and Q-DPBA fluorescence intensity from the QC to the DZ (Fig. 5, a and b). In PSY1-treated roots, K-DPBA and Q-DPBA fluorescence became significantly stronger in the DZ, ~5,300 μm from the QC (Fig. 5, a and b). Because the images used for these profiles were obtained using the middle focal plane of the root, we also measured K-DPBA and Q-DPBA fluorescence intensity using z-stacks covering the complete root width and observed a significant increase in DPBA signal in the DZ (Fig. 5, e and f), while no change was evident in the TZ (Fig. 5, c and d). We observed a similar pattern in the *psyr1,2,3* mutant, in which K-DPBA and Q-DPBA fluorescence accumulated in the DZ without significant changes in the MZ (Fig. S10). These results indicate that PSY1 induces upregulation of genes encoding flavonoid biosynthetic enzymes and accumulation of flavonols in the DZ.

Figure 5

PSY1-dependent flavonol accumulation in root tissue and exudates. a) Five-day-old wt seedling roots were stained with DPBA (2-aminoethyl diphenylboric acid) after 24 h with or without 250 nM PSY1 treatment. DPBA is a probe that allows visualization of Kaempferol (green, K-DPBA) and Quercetin (yellow, Q-DPBA) flavonols. Images are scaled to correspond to the *y*-axis of the plot profile in (b). b) Plot profiles of DPBA fluorescence in 5-d-old wt seedlings grown with or without PSY1 250 nM for 24 h. Data are mean ± SEM. of $n = 12$ seedlings. The asterisk at ~5,300 μm from the QC represents the shortest distance at which the values for K and Q-DPBA fluorescence in the presence of PSY1 became significantly different ($P < 0.05$) from the controls as determined by unpaired 2-tailed Student's *t*-test. The fluorescence intensity of K-DPBA and Q-DPBA was quantified in the TZ (c and d) and in the DZ (e and f) using sum projections generated from 30 and 50 z-section images, respectively, for each region. In (c) and (e), the fluorescence intensity is plotted as a fold change relative to the control. The data shown are box and whisker plots combined with scatter plots; each dot represents an independent seedling measurement. The box spans the interquartile range (25th to 75th percentiles), the center line denotes the median, and whiskers extend to the smallest and largest observed values. Representative images of 2 independent experiments ($n = 10$ to 12 seedlings/experiment) are shown. In (c) different letters indicate significant differences, as determined by 1-way ANOVA followed by Tukey's multiple comparison test ($P < 0.05$). In (e), different letters indicate significant differences as determined by Brown–Forsythe and Welch ANOVA followed by Dunnett's T3 multiple comparisons test ($P < 0.05$). (g) PCA of Arabidopsis root exudate features performed using normalized peak height data acquired by hydrophilic interaction liquid chromatography in positive ionization mode (filtered features, $n = 1{,}077$). Each symbol represents an individual biological replicate; blue symbols denote 6-d-old wt seedlings transferred to mock plates, whereas magenta symbols represent 6-d-old wt seedlings transferred to plates supplemented with 250 nM PSY1 for 24 h before exudate collection. (h) Feature-based molecular networking of flavonol compounds by NPClassifier was generated using GNPS-annotated features (MQScore > 0.7). Node colors reflect the $\log_2$ fold change (PSY1-treatment vs. mock), with white nodes present in the network but not detected in Arabidopsis exudates. Black-bordered nodes indicate compounds that are not significantly increased by the treatment, while red-bordered nodes highlight significantly increased flavonols. In (h), *P*-values are calculated by a 2-tailed Student's *t*-test. The purple arrowheads mark the position of the QC, the pale orange arrowheads mark the end of the meristem, where cells start to elongate, and the magenta arrowhead points to the first root hair bulge, defined as stage +2, indicating the end of the elongation zone in the epidermis. For presentation purposes, images in (a) were placed on a uniform background to standardize panel shape. Individual tiles were acquired and then combined using the LSCM merging function to generate the final complete root images in (a).**[AQ26][AQ27]**

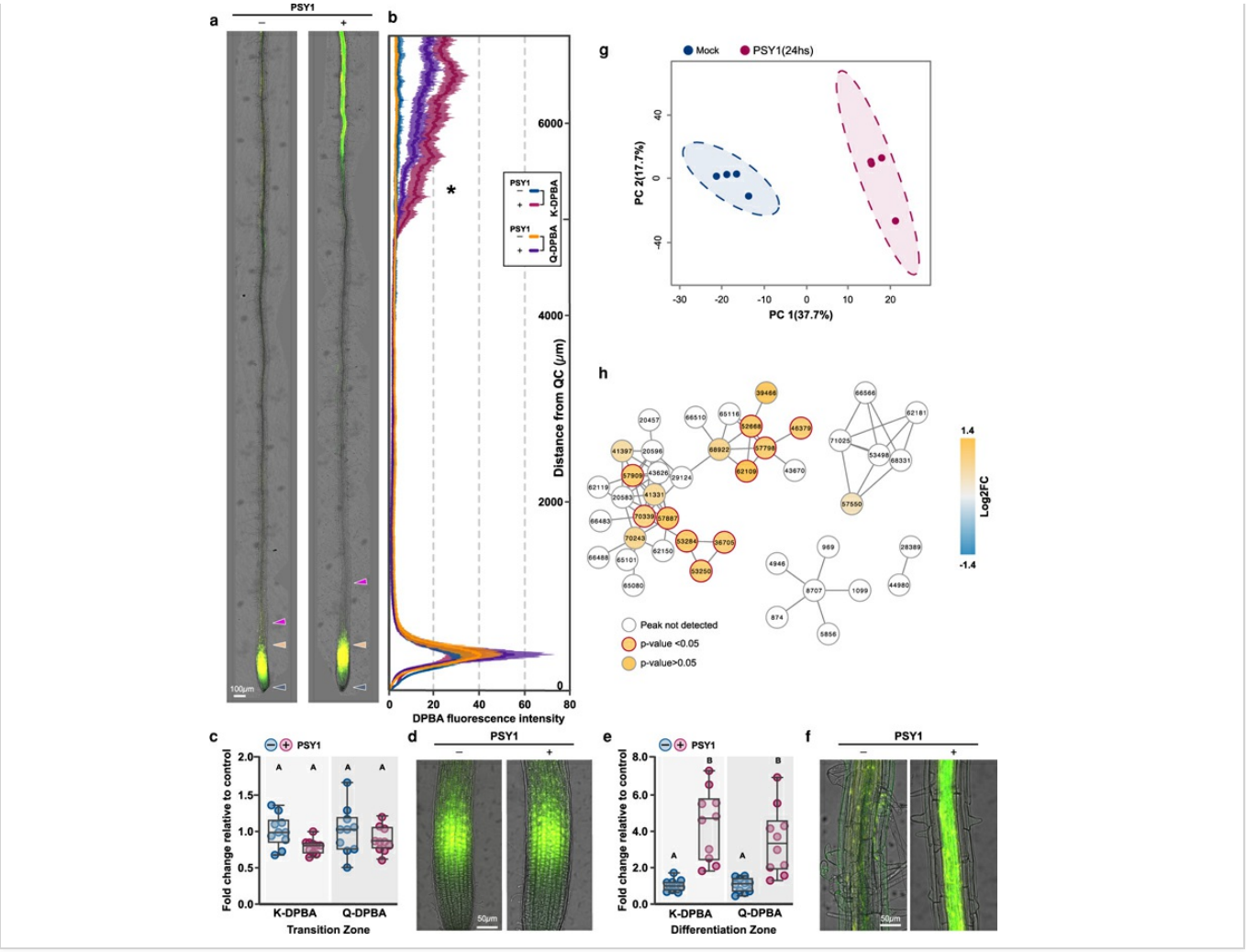

To validate and complement the DPBA staining results, root exudates were collected from 6-d-old wt seedlings grown for 24 h on plates with or without synthetic PSY1. Because root exudates are derived from the root tissues, we have extracted metabolites from the media using methanol and profiled them on an LC-MS/MS platform (Data Set S5). Principal component analysis (PCA) of 1,077 filtered features from LC MS/MS performed using hydrophilic interaction liquid chromatography (HILIC-Z) in positive ionization mode, revealed distinct clustering between exudates from mock and PSY1-treated samples (PERMANOVA $R^2 = 0.372$, $F = 3.549$, $P = 0.02$; Fig. 5g). Further analysis identified features with annotation, defined by an MQScore (cosine score) > 0.7 against a Global Natural Products Social Molecular Networking (GNPS) reference library, and from these we focused on features that NPClassifier putatively assigns to "Flavonols," "Flavones," or "Flavanones" (Data Set S6). This process yielded 27 features used to construct a molecular network (Data Set S7), in which nodes were color-coded based on the average peak height Log_2fold change between PSY1-treated and control samples. In Arabidopsis exudates, 16 of these features were detected, all of which were enriched in PSY1-treated samples, with 10 showing statistically significant differences (*t*-test, $P < 0.05$; Figs. 5h and S11). These features were absent in exudates collected from *tt4-11* mutants, which harbor a mutation in the *CHALCONE SYNTHASE* gene, providing further evidence of the chemical identity of these features (Fig. S11). Additionally, exudates from 7-d-old *Pro35S:PSY1* seedlings accumulated significantly higher levels of the same features compared with wt, whereas the *psy1* exhibited a non-significant trend toward reduced levels (Fig. S11). Comparable results were obtained using HILIC-Z in negative ionization mode and reverse-phase C18 chromatography in both positive and negative ionization modes (Data Sets S5 to S8 and Fig. S12). Combining all these data, the final annotated list includes putative flavonols such as quercetin, kaempferol, and isorhamnetin, with diverse glycosylation patterns, for instance, kaempferol-3-O-glucoside-7-O-rhamnoside, Quercetin 3-(2-glucosylrhamnoside), and isorhamnetin-3-O-rutinoside (Data Set S8). These features were further validated using standards through targeted metabolomic analysis (Data Sets S9 and S10). Thus, PSY1 up-regulation of flavonoid biosynthetic genes is associated with increased flavonoid accumulation in roots, as indicated by a stronger DPBA signal, and further supported by elevated levels of glycosylated flavonols detected in root exudates

Flavonol biosynthesis is required for PSY1-induced root growth

We then explored whether PSY1 could enhance root growth in flavonoid-deficient mutants, also known as *transparent testa (tt)*, due to their seed coat color phenotype (Appelhagen et al. 2014). We tested 4 out of 11 flavonoid pathway genes that were upregulated by

PSY1 treatment in our RNA-seq dataset (Fig. 3). The selection included Col-0 plants with mutations in early flavonoid biosynthesis steps: *tt4-11* (*chs*) and *tt5-2* (*chi*) that lack of flavonoids (Gayomba and Muday 2020), as well as *tt7-7* (*f3′h*), which contains a T-DNA insertion in the gene encoding *F3′H* (Appelhagen et al. 2014) and is known to accumulate only kaempferol. We also examined *myb12*, which carries a mutation in the *MYB12* transcription factor and does not accumulate flavonols in the root (Stracke et al. 2010). We also utilized multiple single- and double-point mutant alleles available in the Ler genetic background, including *85* (*tt4*), *86* (*tt5*), *88* (*tt7*), and *8592* (*tt4tt7*) (Peer et al. 2001; Buer and Djordjevic 2009).

We then generated multiple independent transgenic lines expressing *Pro35S:PSY1* in wt and flavonol-deficient plants in the Col-0 genetic background (Figs. 6 and S13a). The Ler mutants were subjected to synthetic PSY1 treatment (Fig. S14). We found that *PSY1* ectopic expression or synthetic PSY1 treatment led to significantly longer primary roots only in wt seedlings (Figs. 6a, S13e and S14a). Under our growth conditions, the flavonoid biosynthetic enzyme mutants developed longer MZ compared with the wt, as previously observed by Silva-Navas et al. (2016), with the exception of *85 (tt4)* and *8592 (tt4tt7)* in the Ler genetic background providing an example of how identical mutations can yield distinct phenotypes in different genetic backgrounds (Figs. S13, b to d and S14b). In line with our previous finding that PSY1 does not control the position of the TZ, ectopic *PSY1* expression or synthetic PSY1 treatment did not affect the MZ length in both wt and flavonoid-deficient mutants (Figs. S13, b to d and S14b). To validate these results, we also compared MZ cell number in *Pro35S:PSY1* vs. empty vector (EV, as control) in wt and *tt4-11* using a cortical cell length profile (Fig. S13, b and c) and detected no significant changes in the MZ size. Moreover, we found that the cell elongation profiles were almost indistinguishable between *tt4-11* with ectopic *PSY1* expression (*tt4-11-Pro35S:PSY1*) and *tt4-11* with EV. In contrast, *Pro35S:PSY1* expression in a wt background caused a significant increase in mature cell length (Figs. 6, b and c, S4d and S13, b and f). In *tt4-11* and *8592 (tt4tt7)* mutants, mature cortical cells were shorter than in wt, and their size was less responsive to *PSY1* expression (Figs. 6, b and c, S13f and S14, c and d). Despite no significant differences in mature cortical cell length observed among other mutants compared with the wt, we successfully confirmed a consistently reduced response to both *PSY1* overexpression and synthetic PSY1 treatment (Figs. 6, b and c, S13f and S14, c and d). These data suggest that PSY1-mediated control of mature cortical cell size relies on both kaempferol and quercetin accumulation.

Figure 6

Flavonol biosynthesis is required for PSY1 control of root zonation. a) Root elongation rate (mm/h) ($n = 10$ to 15 seedlings), (b and c) mature cortical cell length ($n = 60$ to 80 cells), (d) root tip architecture, (e) distance from the end of the MZ to first root hair bulge at stage +2 (RHB 2+) ($n = 8$ to 10 seedlings), (f) length between consecutive root hairs in 1 trichoblast file ($n = 40$ to 50) in 7-d-old independent homozygous transgenic lines that accumulated higher levels of PSY1 (*Pro35S: PSY1*) with EV control generated in Col-0 and mutant plants defective in flavonol biosynthesis (*tt4-11*, *tt5-2*, *tt7-7*, and *myb12*). Only one homozygous transgenic line overexpressing *PSY1* is included in this figure; 2 more lines with similar results are presented in Fig. S13. In (c), the limits of a representative mature cortical cell are shaded in green. In (c), the image is a single focal plane. In (d), the length between consecutive root hairs in 1 trichoblast file is highlighted in magenta. In (a), (b), (e), and (f), the data shown are box and whisker plots combined with scatter plots; each dot indicates the measurement of the designated parameter listed on the *y*-axis. The box spans the interquartile range (25th to 75th percentiles), the center line denotes the median, and whiskers extend to the smallest and largest observed values. Different letters indicate significant differences, as determined by 1-way ANOVA followed by Tukey's multiple comparison test ($P < 0.05$). The purple arrowheads mark the position of the QC, the pale orange arrowheads mark the end of the meristem, where cells start to elongate, the green arrowheads indicate the mature cortical cell size, and the magenta arrowhead points to the first root hair bulge, defined as stage +2, indicating the end of the elongation zone in the epidermis. For presentation purposes, images in (d) were placed on a uniform background to standardize panel shape.**[AQ28][AQ29]**

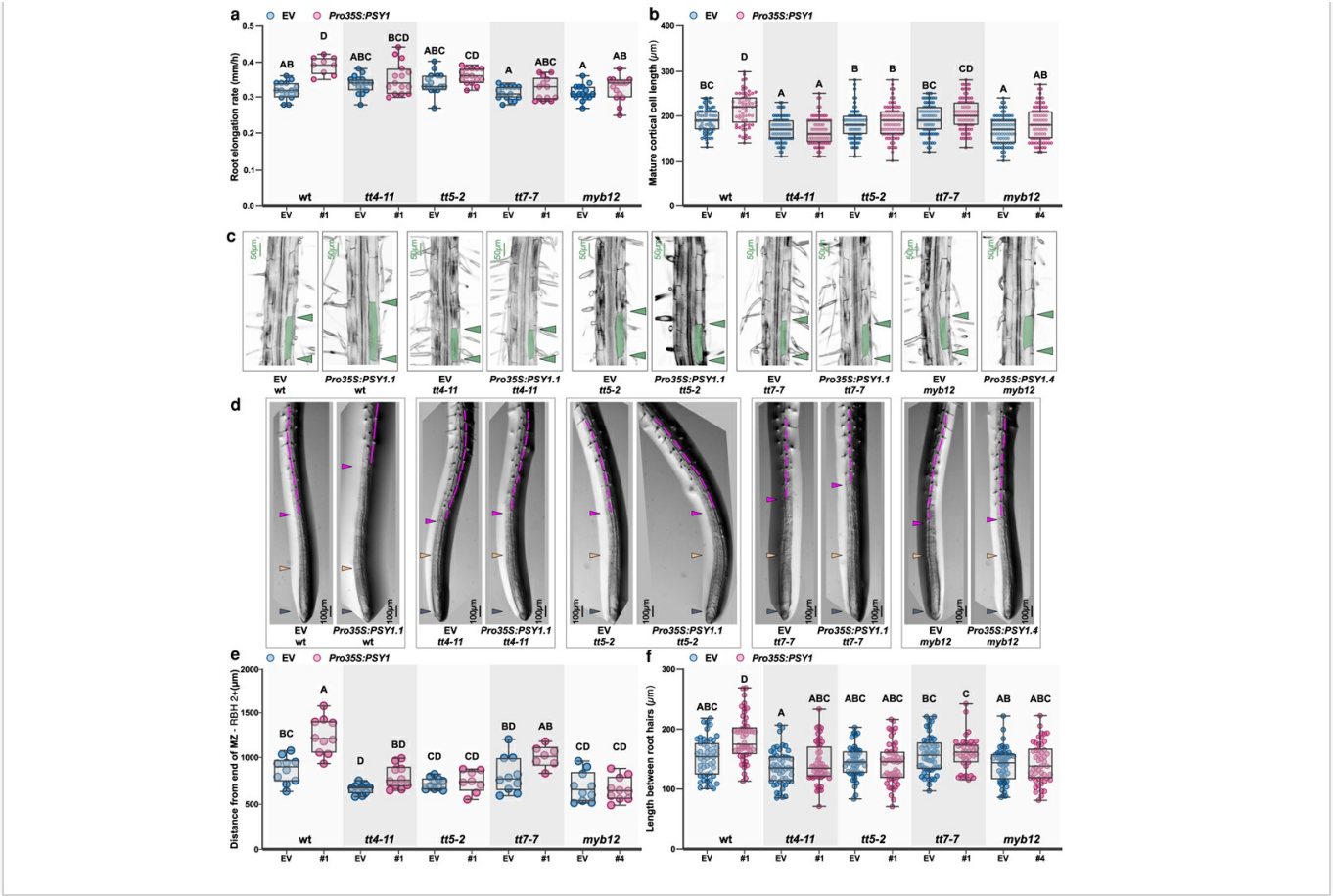

We also observed that in the *tt4-11* mutant, root hairs developed significantly closer to the end of the MZ compared with wt plants (Figs. 6, d and e and S13g). This phenotype was also observed in all flavonol-deficient mutants in the Ler background (Fig. S14e). These findings align with previous studies indicating that *tt4-11* mutants exhibit a higher number of root hairs in a region closer to the TZ (Gayomba and Muday 2020). Gayomba and Muday (Gayomba and Muday 2020) also found that the length between consecutive root hairs in 1 trichoblast file was reduced in *tt4-11* compared with wt; we observed a similar trend. However, under our growth conditions, these results were not statistically significant (Figs. 6, d and f and S13h). Together, these results suggest that morphological signs of differentiation are shifted toward the root tip in flavonol-deficient plants, emphasizing the role of flavonol biosynthesis in proper root zonation. Additionally, when examining root hair initiation, we found that it occurred farther away from the root tip in wt plants expressing *PSY1* ectopically or grown in media supplemented with synthetic PSY1. This significant response was not observed in other flavonoid mutants tested (Figs. 6, d to f, S13, g and h and S14e).

To further validate the requirement of flavonoids for PSY signaling, we examined the genetic interaction between PSY receptors and flavonoid biosynthesis. Because transcriptomic analysis of *psyr1,2,3* roots showed up-regulation of flavonoid biosynthetic genes (Fig. S8e), we generated a quadruple mutant combining *psyr1,2,3* with the flavonoid-deficient allele *tt4-11* (*psyr1,2,3 × tt4-11*). The long-root phenotype observed in *psyr1,2,3* was partially suppressed in the *psyr1,2,3 × tt4-11* mutant (Fig. S15a). Cellular analysis further revealed that these plants exhibited a longer MZ compared with wt, similar to *tt4-11* (Fig. S15, b and c). Moreover, the *psyr1,2,3 × tt4-11* mutant was indistinguishable from wt when we measured the distance from the end of MZ to the first root-hair bulge at stage +2, the distance between consecutive root hairs within a trichoblast file, and the length of mature cortical cells (Fig. S15, d to h). Together, these genetic interactions indicate that flavonoid accumulation is required for PSY signaling mediated by PSYR receptors.

Synthetic naringenin treatment phenocopies PSY1 treatment

To test the role of flavonols in root zonation, we treated plants with naringenin, a flavonoid precursor, and compared them with plants treated with PSY1. We hypothesized that increasing flavonol levels in the DZ would mimic the effects of *PSY1* overexpression.

First, we confirmed that naringenin could be converted to different flavonol products in *tt4-11* roots by detecting the K-DPBA and Q-DPBA signals and comparing those values to a wt plant (Fig. S16a). For this, we tested a range of concentrations of naringenin (10, 25, or 50 μM) and found that K- and Q-DPBA signals increased in response to the higher concentrations of synthetic naringenin supplied to the plants, reflecting a dose-dependent accumulation of flavonols (Fig. S16b). Next, we examined whether naringenin could rescue root elongation defects in the *tpst-1* mutant as PSY1 does. For this experiment, we transferred 5-d-old *tpst-1* seedlings to plates with different concentrations of naringenin (10, 25, or 50 μM) or PSY1 (50 nM) and measured root elongation after 48 h. Although all

naringenin treatments increased root length compared with untreated controls, the strongest and significant effect was observed at 25 μM (Fig. S16c).

We then analyzed the cell length profile of *tpst-1* cortical cells from the QC to the DZ and observed a striking similarity between PSY1 and 25 μM naringenin treatments (Fig. S16, c and d). It has been previously shown that 8-d exposure to quercetin significantly reduced root meristem size in the wt background (Silva-Navas et al. 2016). However, we found that none of the treatments altered the size of the MZ in *tpst-1*, indicating that under these conditions, naringenin did not affect the position of the TZ in this mutant background (Fig. S16d). To examine how naringenin affects cell elongation in *tpst-1* mutants, we measured the mature cortical cell length and the length between consecutive root hairs in 1 trichoblast file in *tpst-1* plants treated with 25 μM naringenin. We found that both parameters increased, mimicking the effects of PSY1 treatment in this mutant (Figs. 7, a to d and S16, e and f). In agreement with the root elongation results, 10 and 50 μM naringenin treatment produced intermediate phenotypes: although significantly different from wt, their effects on distance between root-hair and mature cortical cell length did not reach the magnitude observed with 25 μM naringenin or PSY1 treatment (Fig. S16, e and f). These results suggest that either naringenin itself or the flavonols accumulated upon naringenin treatment can act downstream of the PSY1 signaling pathway to control the magnitude of cell elongation.

Figure 7

Exogenous treatment with naringenin rescues cell expansion defects in *tpst-1*. a and b) Mature cortical cell length ($n = 50$ cells), (c) root tip architecture, and (d) length between consecutive root hairs in 1 trichoblast file ($n = 100$ cells) in 5-d-old wt and *tpst-1* seedlings grown for 48 h in control conditions (−) (either 1×MS or 1×MS supplemented with EtOH) or treated with 50 nM PSY (+) or 25 μM naringenin (+). In (a), the limits of a representative mature cortical cell are shaded in green. This image is a single focal plane. In (c), the length between consecutive root hairs in 1 trichoblast file is highlighted in magenta. In (b) and (d), the data shown are box and whisker plots combined with scatter plots; each dot indicates the measurement of the designated parameter listed on the *y*-axis. The box spans the interquartile range (25th to 75th percentiles), the center line denotes the median, and whiskers extend to the smallest and largest observed values. Different letters indicate significant differences, as determined by 1-way ANOVA followed by Tukey's multiple comparison test ($P < 0.05$). The purple arrowheads mark the position of the QC, the green arrowheads indicate the mature cortical cell size, and the magenta arrowhead points to the first root hair bulge, defined as stage +2, indicating the end of the elongation zone in the epidermis. For presentation purposes, images in (c) were placed on a uniform background to standardize panel shape.[AQ30][AQ31]

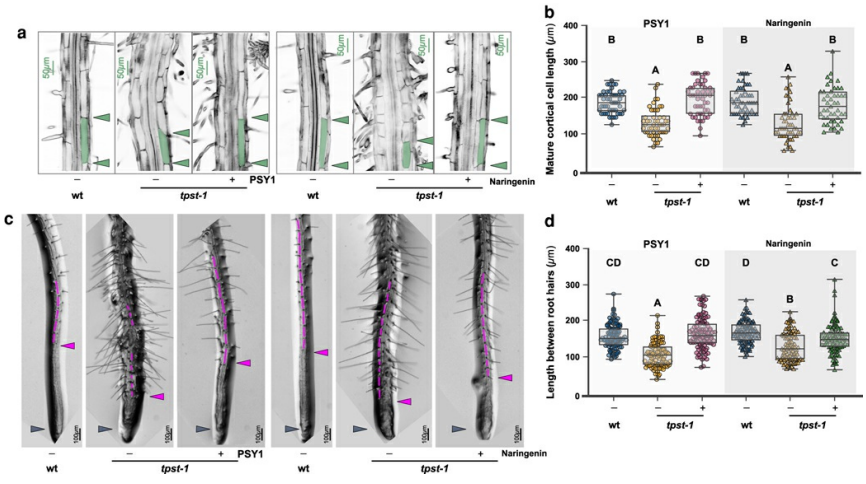

Changes in PSY1 signaling alter auxin-induced gene expression and H_2O_2 accumulation

Our results indicated that PSY1-induced root growth required flavonol biosynthesis in the DZ. We next looked for potential flavonol targets involved in this process. Flavonols are known to affect root growth through 2 mechanisms: regulation of PAT through inhibition of PIN-mediated auxin efflux and maintenance of ROS homeostasis (Daryanavard et al. 2023). Based on these reports, we assessed whether PSY1 abundance altered either of these processes.

We first assessed possible changes in ROS quantity or distribution in response to PSY1 signaling using nitro blue tetrazolium (NBT) staining to detect O^{2-} and BES-H_2O_2-Ac fluorescence to detect H_2O_2 (Yamada et al. 2020). We used RGF1-treated plants as a control because RGF1 is known to alter ROS accumulation to control MZ size (Yamada et al. 2020). RGF1 increased total NBT intensity in the MZ (Fig. S17, c and d), but loss or ectopic expression of *PSY1* in *psy1* or *Pro35S:PSY1*, respectively, did not affect NBT intensity

(Fig. S17, a to d). These results provide further evidence that PSY1 does not regulate MZ size in a ROS-dependent manner. It has been proposed that flavonol modulation of ROS accumulation is one of the mechanisms driving root hair initiation (Gayomba and Muday 2020). We, therefore, hypothesized that PSY1 signaling may affect root hair development by modulating H_2O_2 levels in the root epidermis. To test this, we measured H_2O_2 accumulation in the epidermis along the root longitudinal axis using BES-H_2O_2-Ac. We compared BES-H_2O_2-Ac fluorescence intensity in wt, *psy1*, *Pro35S:PSY1*, and RGF-treated plants. RGF1 treatment led to a longer MZ with lower BES-H_2O_2-Ac fluorescence intensity compared with the untreated control (Fig. S17, e and f; Yamada et al. 2020). In contrast, we found that *Pro35S:PSY1* plants had lower H_2O_2 levels than wt plants, while *psy1* plants had higher H_2O_2 levels, although the overall H_2O_2 epidermal profile remained the same as wt (Figs. 8, a and b and S18a). Notably, the effect of *Pro35S:PSY1* is lost in *tt4-11*, indicating that the ability of PSY1 to control ROS accumulation in the epidermis requires flavonol biosynthesis (Figs. 8, c and d and S18b).

Figure 8

PSY1 reduction of H_2O_2 accumulation in the epidermis requires flavonoid biosynthesis. (a and c) Representative epidermal H_2O_2 accumulation along the root longitudinal axis using BES-H2O2-Ac (BES) of *psy1*, wt, and *Pro35S:PSY1* (a) and *tt4-11*×EV, *tt4-11*×*Pro35S:PSY1-1* and *tt4-11*×*Pro35S:PSY1-4* (c) 6-d-old seedlings. BES fluorescence intensity profile is shown using RGB-rainbow false color with its color scale bar; organ boundaries are marked by white dashed lines. In (a) and (c), images are scaled to correspond to the *y*-axis of the plot profile in (b) and (d). b and d) Plot profiles of epidermal BES fluorescence in *psy1*, wt, and *Pro35S:PSY1* (b) and *tt4-11*×EV, *tt4-11*×*Pro35S:PSY1-1* and *tt4-11*×*Pro35S:PSY1-4* (d) 6-d-old seedlings. Data are mean ± SEM. of $n = 13$ to 15 seedlings. For presentation purposes, images in (a) and (c) were placed on a uniform background to standardize panel shape. Individual tiles were acquired and then combined using the LSCM merging function to generate the final complete root images in (a) and (c).**[AQ32]**

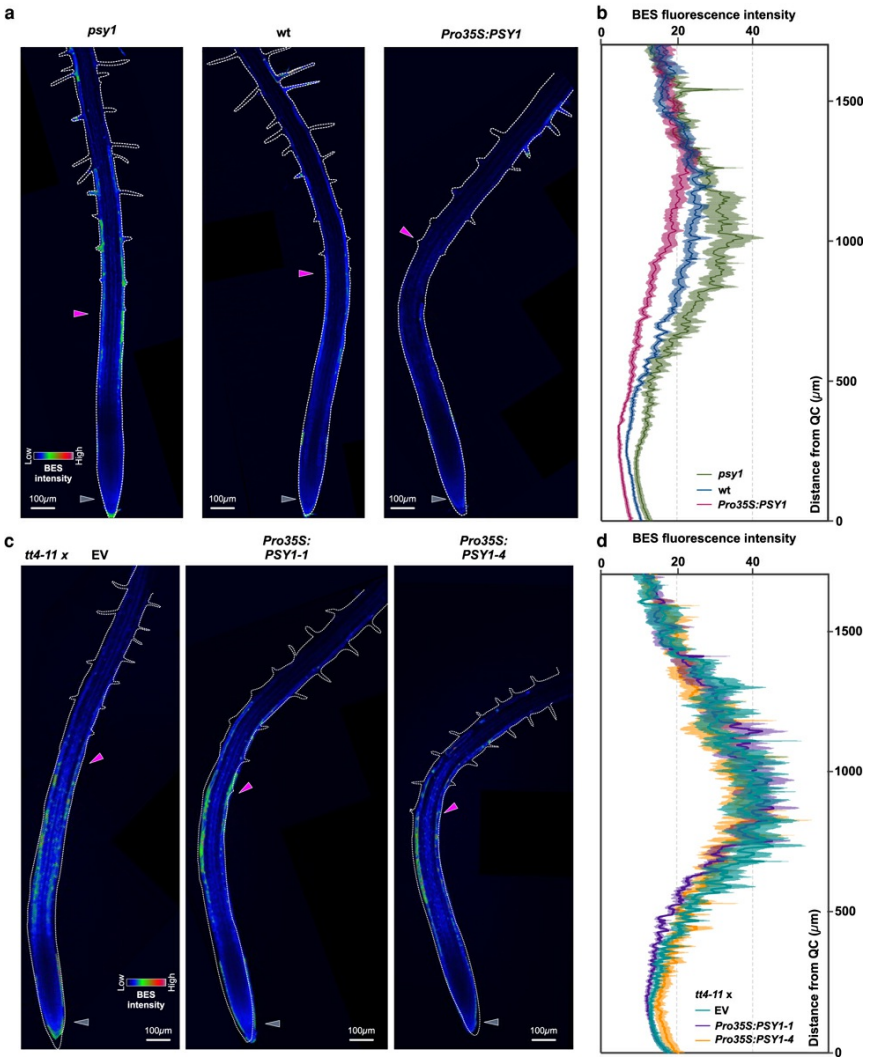

We then examined the effect of PSY1 on auxin-induced gene expression in the root stele with the *DR5v2:3nGFP* reporter (Liao et al. 2015). In agreement with previous observations, a 6-d treatment with synthetic PSY1 did not alter auxin-induced gene

expression in the meristem (Figs. 9, a and c, S7, e and f). Similarly, *DR5v2:3nGFP* expression in the meristem zone of the *psy1* mutant was unchanged compared with wt (Fig. 9, b and d). Notably, synthetic PSY1 treatment reduced *DR5v2:3nGFP* signal in the stele starting ~1,500 μm from the QC; in contrast, in the *psy1* mutant, reporter expression was increased (Fig. 9, a to d). Given that elevated auxin levels can lead to cell wall alkalization and inhibit cell elongation (Barbez et al. 2017; Serre et al. 2023), we hypothesize that increased *DR5v2:3nGFP* activity in the *psy1* mutant signals a halt in cell growth, whereas reduced *DR5v2:3nGFP* expression in the EZ/DZ of PSY1-treated roots promotes continued elongation, ultimately yielding mature cell sizes that differ significantly from those of wt plants (Figs. 1, d and g, S4, d to h).

Figure 9

PSY1 treatment alters auxin-induced gene expression in the stele. a and b) Activity of the auxin response reporter line, *DR5v2:n3GFP* (yellow) in 6-d-old roots grown in the presence or absence of 100 nM PSY1 (a) and in *psy1* compared with wt (b). (Left) Longitudinal cross-sections of the roots; organ boundaries are marked by white dashed lines. (Right) Magnified images of *DR5v2::n3GFP* expression in the stele in the DZ are highlighted by a red box (3,000 to 3,500 μm from the QC). c and d) Changes in *DR5v2::n3GFP* expression in response to PSY1 treatment (c) and *psy1* background (d) in the stele along the root longitudinal axis from the QC (0 μm) to the DZ (3,500 μm). The sizes of the different developmental zones measured in the root cortex are depicted in blue and pink for plants grown without and with PSY1 (c) and in blue and green for wt compared with *psy1* (d), respectively. In (c and d), fluorescence intensity is plotted as a fold change relative to the control. The data shown are box and whisker plots combined with scatter plots; each dot represents an independent seedling measurement. The box spans the interquartile range (25th to 75th percentiles), the center line denotes the median, and whiskers extend to the smallest and largest observed values. Representative images of 4 independent experiments ($n = 8$ to 12 seedlings/experiment) are shown. *P*-values are calculated by a 2-tailed Student's *t*-test. For presentation purposes, images in (a) and (b) were placed on a uniform background to standardize panel shape. Individual tiles were acquired and then combined using the LSCM merging function to generate the final complete root images in (a) and (b).**[AQ33][AQ34][AQ35]**

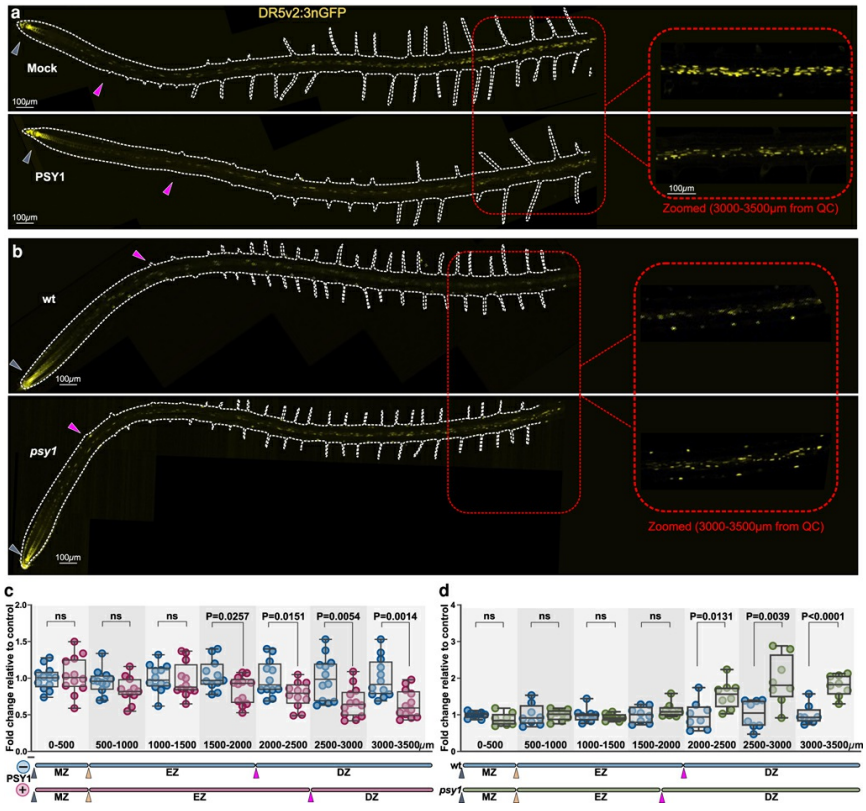

Discussion

Root zonation is the spatial arrangement of the cells along the root longitudinal axis, reflecting the balance between cellular growth and maturation (Fig. 1a, left side of the panel). The sustained growth of the root requires these processes to be tightly coordinated. Previous studies have shown that several phytohormone and peptide signaling pathways regulate the establishment of boundaries that separate cells in different developmental stages in the root, therefore controlling root zonation (Hsiao and Yamada 2021; Zluhan-Martínez et al. 2021). Here, we demonstrate that the peptide hormone PLANT PEPTIDE CONTAINING SULFATED TYROSINE 1 (PSY1) signals the developmental-specific accumulation of flavonols to reshape root zonation by promoting enhanced

cell elongation with a shootward displacement of characteristics common to mature cells. A schematic summary of these effects is presented in Fig. 10.

Figure 10

A diagram summarizing the observed effects of increased levels of PSY1 in the root. Accumulation of PSY1 is correlated with enhanced root growth, primarily via a significant increase in mature cell size. Moreover, in plants with elevated PSY1 levels, morphological changes associated with cell differentiation, such as root hair initiation, are observed further away from the root tip. Our results suggest that PSY1 activates flavonol biosynthesis in the DZ and promotes the accumulation of various flavonol glycosides in root exudates. Notably, these secondary metabolites are required for the PSY1-mediated reduction of H_2O_2 levels in the epidermis of both the EZ and DZ. Additionally, we observed a concurrent decrease in auxin-induced gene expression within the DZ stele. In the figures, purple arrowheads indicate the position of the QC, the pale orange arrowheads mark the end of the meristem, where cells start to elongate, and the magenta arrowheads mark the end of the EZ, as defined by the emergence of root hairs.[AQ36][AQ37]

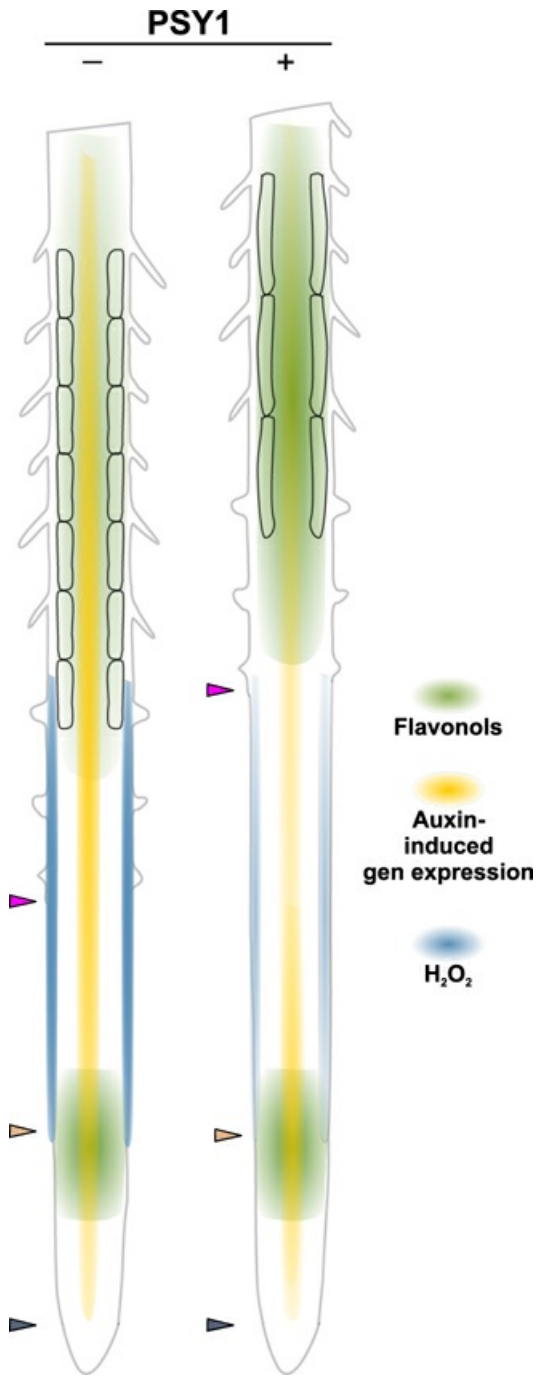

The PSY family has been shown to participate in the control of cortical mature cell size in Arabidopsis primary roots (Amano et al. 2007; Ogawa-Ohnishi et al. 2022). Despite recent progress in characterizing the LRR-RLKs involved in peptide perception, the biological processes triggered by PSYs remain largely unexplored. In this study, we focused on one of the members of this family, PSY1. We

started by investigating the function of PSY1 in root zonation based on a detailed cell length profile analysis (Fig. 1d). We observed that *psy1* mutants have shorter mature cells in both the root cortex and epidermis, leading to reduced root growth (Fig. 1, h and k). Additionally, we found that defining mature cell features, such as root hair initiation and deposition of secondary cell wall in the protoxylem, which marks the cessation of rapid cell elongation (Le et al. 2004; Li et al. 2022), emerged closer to the root tip in *psy1* plants than in wt plants (Fig. 1, i to m). These phenotypes could be reversed when synthetic PSY1 is supplemented exogenously and are also observed in *psyr1,2,3* triple mutant, which is insensitive to PSY1 treatment (Figs. 1, i to m and S6; Ogawa-Ohnishi et al. 2022). Overall, PSY1 signaling regulates root growth by modulating the magnitude that cells elongate before reaching their final, differentiated size.

Given that our analysis is based on cell length, without specific data on growth rates, the exact effect of PSY1 on these observed phenotypes remains to be fully understood. It is possible that PSY1 signaling is (i) controlling the maximum cellular growth rate, which is the speed at which cells elongate before leaving the rapid growth region; (ii) determining the onset of growth cessation or the position at which the cellular growth rate began to decrease shootward in the EZ; or (iii) influencing a combination of both. Finally, it is worth noting that the overall progression to the root maturation was affected by PSY1 signaling, including tissues such as the epidermis where the expression of *PSY1* promoter was barely detected (Figs. 1a and S1, b and d). This observation aligns with the secreted and diffusible nature of these peptides, potentially creating a gradient from their site of synthesis. Consequently, the expression pattern of *ProPSY1-GFP* might not accurately represent the regions where PSY1 is active and perceived by its extracellular receptors which exhibit broad expression across Arabidopsis root tissues(Ogawa-Ohnishi et al. 2022; Wang et al. 2022; Fig. S2).

The role of PSY1 in controlling developmental transitions was previously described at the onset of the embryo-to-seedling transition, which is associated with the establishment of a well-sealed cuticle required for an aerial lifestyle. In the model proposed by De Giorgi et al. (2021), tyrosine-sulfated peptides, including PSY1, are released toward the embryo as part of the endosperm secretome to signal the formation of the seedling cuticle. In agreement with this model, *psy1* and endosperm-less seedlings had higher toluidine blue O uptake in cotyledons, suggesting cuticle defects in these plants (De Giorgi et al. 2021). Transcriptomic analysis revealed that in the presence of light, GO categories such as flavonoid and glucosinolate biosynthetic processes were enriched among repressed genes in endosperm-less seedlings relative to wt (De Giorgi et al. 2021). If we consider the lack of endosperm as a proxy for reduced PSY1 signaling in the developing seedling, this analysis supports a role for PSY1 in controlling the onset of the embryo-to-seedling transition through the expression of genes involved in specialized metabolite biosynthesis.

The transcriptomic data generated in this study revealed that synthetic PSY1 treatment of Arabidopsis seedling roots increased expression of genes in the phenylpropanoid and flavonoid biosynthetic pathways (Fig. 3 and Data Set S1). Similarly, the triple PSY receptor mutant (*psyr1,2,3* or *tri-1*) also exhibited increased expression of genes that encode flavonol biosynthetic enzymes (Fig. S8e; Wang et al. 2022). Consistent with these results, *psyr1,2,3* and *PSY1* overexpression plants both developed longer roots (Figs. S4, b and c, S6, a and b; Ogawa-Ohnishi et al. 2022; Wang et al. 2022). It is worth noting that more flavonol pathway genes are differentially expressed in the triple receptor mutant compared with our synthetic PSY1 treatment. For example, in the *FLAVONOL SYNTHASE* (*FLS*), *4-COUMARATE: COA LIGASE* (*4CL*), and *PHENYLALANINE AMMONIA-LYASE* (*PAL*) gene families, only one isoform was activated by PSY1 treatment, while multiple isoforms were upregulated in the triple receptor mutant. Also, *O-METHYLTRANSFERASE 1* (*OMT1*), involved in the methylation of flavonols to generate isorhamnetin (Saito et al. 2013), for which we did not find changes after PSY1 synthetic treatment, is activated in the triple receptor mutant background, indicating that *PSY* genes may also regulate the accumulation of isorhamnetin scaffolds. In support of this hypothesis, root exudates collected from PSY1-treated wt seedlings showed significant enrichment of features identified as isorhamnetin and isorhamnetin-3-O-rutinoside using targeted metabolomic analysis (Data Sets S9 and S10). The metabolomic data supporting these results were obtained from root exudates. Future work will examine root tissue metabolites, which would further support our results. Accumulation of flavonoids is also observed in the exudate of rice plants that accumulate higher levels of OsPSY (Shi et al. 2026). KEGG pathway analysis of the triple PSYR mutant also revealed enrichment for genes that participate in glucosinolate biosynthesis, including glucosinolates derived from methionine and aromatic amino acids, which were not detected in the PSY1 treatment (Fig. S8e). The crosstalk between glucosinolate biosynthesis and flavonols has been recently explored by Naik et al. (2024) as part of an effort to understand the molecular mechanisms underlying the ability of flavonols to control plant development. Transcriptomic and targeted metabolomic analysis hint at flavonols promoting the accumulation of aliphatic glucosinolates (Naik et al. 2024). Although our study did not assess changes in glucosinolate biosynthetic enzymes, it would be interesting to test if PSY1 affects this metabolic pathway using root samples generated after longer PSY1 synthetic treatment or in the *psy1* mutant.

It was recently shown that CLE-LIKE6 (CLEL6), a member of a different family of small tyrosine-sulfated peptides, inhibits the biosynthesis of anthocyanin, another type of flavonoid (Bühler et al. 2023). *CLEL6* expression in the hypocotyl decreases during photomorphogenesis, which activates anthocyanin biosynthesis genes and leads to pigment accumulation. These pigments help regulate ROS levels and facilitate seedling development during de-etiolation (Bühler et al. 2023). The contrasting effects of PSY1 and CLEL6

may be due to tight spatial control of flavonoid enzyme gene expression, which allows only flavonols, not anthocyanins, to accumulate in roots. In support of this idea, we found that PSY1 upregulates MYB12, a flavonol-specific flavonoid regulator (Stracke et al. 2007), but does not affect *PRODUCTION OF ANTHOCYANIN PIGMENT1 (PAP1)*, which controls late anthocyanin biosynthesis genes (Fig. 4 and Data Set S1; Xie et al. 2006). On the other hand, exogenous postharvest application of PHYTOSULFOKINE (PSK) has been shown to delay senescence and promote the accumulation of flavonoids and phenylpropanoids in strawberry fruit by activating key biosynthetic enzymes, including *PAL* and *CHS* (Aghdam et al. 2021). These findings suggest that PSY and PSK signaling may converge on common redox- and flavonoid-associated pathways to coordinate growth and postharvest responses, highlighting the broader integration of sulfated peptide signaling and plant metabolism.

The results presented in this paper shed light on how flavonols accumulate in a developmental zone-specific manner during root development. One of the few examples of a root growth modulator affecting the flavonoid pathway is the transcription factor WRKY23 (Grunewald et al. 2012). Specifically, WRKY23 induces *FLAVONOID 3-HYDROXYLASE* (*F3′H*) expression to negatively influence auxin transport from the shoot to the root. Overexpression of WRKY23 leads to higher flavonol levels in the whole root, including TZ and DZ, reducing rootward auxin transport and causing root tip disorganization. Accumulation of flavonols in the TZ has also been studied in detail by Silva-Navas et al. (2016). In this case, flavonols reduce auxin activity in the MZ and decrease *PLT* gene expression, providing a mechanism to explain their role as inhibitors of root growth. Given that PSY1-induced root growth requires the activation of flavonoid biosynthetic enzymes and flavonol accumulation, specifically in the DZ as detected by DPBA staining, we surmised that the effect of flavonols on root growth depends on where they accumulate within the root. To test this hypothesis, we used *tpst-1*, a mutant in which synthetic flavonol treatment does not modify MZ size. Because *tpst-1* plants have a shorter MZ (Matsuzaki et al. 2010; Yamada et al. 2020), as a result of decreased PLT protein stability, it is possible that any additional increase in flavonol levels will not further inhibit meristematic activity. Complementation of cell elongation defects in *tpst-1* by naringenin likely reflects the effects of flavonols in the DZ, phenocopying the effects of the PSY1 signaling pathway (Figs. 7 and S16, c and d).

Auxin-induced gene expression measurement using a response reporter line (*DR5v2:3nGFP)* showed a marked reduction at 1,500 μm from the QC between PSY1-treated roots as compared with untreated roots (Fig. 9, a and c). This point coincides with the location where cortical cells of untreated plants stop growing whereas cells continue to elongate in PSY1-treated plants (Figs. 1d, S4d and S5d). We also observed a significant increase in the activity of *DR5v2:3nGFP* in the DZ in the *psy1* genetic background (Fig. 9, b and d). We hypothesize that changes in flavonol accumulation in the DZ in response to PSY modifies auxin transport from the shoot, resulting in changes in auxin activity in the EZ. Moreover, the extended elongation phase observed in plants with high PSY1 levels might be due to a delayed onset of growth cessation. It is known that the cell wall-altering properties of cytokinin requires an increase of auxin levels in the EZ (Street et al. 2016; Liu et al. 2022).

To further test whether flavonoids are required for PSY signaling, we crossed the *psyr1,2,3* triple receptor mutant with the flavonoid-deficient allele *tt4-11*, generating a quadruple mutant (*psyr1,2,3 × tt4-11*). These genetic interactions indicated that flavonoid accumulation is required for PSY signaling mediated by PSYR receptors (Fig. S15). However, the fact that the *psyr1,2,3 × tt4-11* mutant does not fully phenocopy *tt4-11* suggests that flavonoids are not the only downstream components contributing to PSY responses. Consistent with this, transcriptomic analysis revealed enrichment of additional signaling pathways among the downregulated KEGG categories, including the “MAPK signaling pathway” and “plant hormone signal transduction” (Fig. 3e and Data Set S1). The transcripts related to these pathways included *PYL4*, *PYL5*, and *PYL6*, which are members of the *PYRABACTIN RESISTANCE1* (*PYR1*)/*PYR1-like* (*PYL*)/*REGULATORY COMPONENTS OF ABA RECEPTOR* (*RCAR*) family of proteins involved in ABA perception (Zhao et al. 2018). Also, the *1–AMINOCYCLOPROPANE-1–CARBOXYLATE (ACC) OXIDASE 1* (*ACO1*), which oxidases ACC to ethylene (Markakis et al. 2012), was downregulated. It is known that ABA and ethylene signals are integrated to mediate root growth inhibition (Luo et al. 2014). PSY1 suppression of these hormonal pathways is consistent with the shootward displacement of differentiation signs. Thus, genetic interactions between PSY1 and ABA and ethylene pathways can be assessed for their effects on the transition from active growth to differentiation.

Although it has been shown that the PSY-PSYR signaling pathway mediates the trade-off between growth and stress responses in various plant species (Ogawa-Ohnishi et al. 2022), the specific roles of each PSY peptide and PSYR in this process remain largely unknown. Our results show that PSY1 may act as a repressor of growth cessation through modulation of flavonols, which are known to control plant growth and stress responses by acting as ROS scavengers (Taylor and Grotewold 2005; Brunetti et al. 2018). In roots flavonols modulate ROS to control root hair formation (Daryanavard et al. 2023). In the proposed model, cortical cells that accumulate flavonols exhibit low ROS levels, whereas trichoblasts display higher ROS levels and reduced flavonol accumulation. In *tt4* mutants, which lack flavonol biosynthesis, root hairs develop closer to the root tip, and there is a higher frequency of trichoblast cells (Gayomba and Muday 2020). Together, these results support a model in which flavonols modulate root hair formation by spatially controlling ROS in the Arabidopsis root epidermis. We observed that in plants ectopically accumulating PSY1, there was a shootward displacement in root hair development (Fig. S4, i to k), and this phenotype was absent when PSY1 was overexpressed in a background

deficient in flavonoid accumulation (Figs. 6e and S13g). In agreement with these phenotypes, we found that increased PSY1 signaling reduced H_2O_2 levels in the EZ, an effect that was lost in *tt4-11* mutant background, which does not produce flavonoids (Fig. 8, c and d).

Altogether, our findings establish a mechanistic link between tyrosine-sulfated peptide signaling and spatial reprogramming of flavonol biosynthesis that governs root development in Arabidopsis (Fig. 10).

Materials and methods

Plant materials, growth conditions, and treatments

A. thaliana accession Col-0 was used throughout this study as the wt background, unless otherwise indicated. See Tables S1 and S2 for a full list and description of the mutants and reporter lines utilized in this study. Seeds were surface sterilized using 70% ethanol for 10 min and then rinsed 3 times with absolute ethanol. Seeds were stratified in 0.1% agarose at 4 °C for 3 d before germination. Plates were prepared with standard MS medium (1× Murashige and Skoog salt mixture with vitamins, MSP09-Caisson Laboratories), 1% sucrose, and 0.3% gellan gum (G024-Caisson-Gelzan) and adjusted to pH 5.65 with KOH. Seeds were placed on the plates (20 seeds per plate), and the lids were secured with Micropore surgical tape (1530-0). Seedlings were grown in vertically positioned plates in a chamber with long photoperiods (16 h light/8 h dark) at 21 °C. Germination rate was scored in every experiment, and no significant differences between genotypes and treatments were observed.

For synthetic peptide treatments, peptide (or water for untreated plants) was added to the MS media before pouring it into a plate. The length and concentration of the peptide treatment are specified in the figure legends. Seedlings were either germinated on media or moved after germination to treatment plates. All peptides used in the experiments are tyrosine sulfated. The synthetic PSY1 peptide lacks the hydroxy- and L-Ara3- modifications at the C-terminus and was obtained from Pacific Immunology (Ramona, CA, USA). RGF1 was obtained from Peptide 2.0 (Chantilly, VA, USA). Peptides were diluted in ddH_2O to a final concentration of 1 mM. For synthetic flavonoid treatments, plants were grown on 1× MS media prepared as described above for 5 d and subsequently moved to 1× MS medium containing different concentrations of naringenin or ethanol (mock treatment) for 48 h. Stock solutions of naringenin (Indofine Chemical Company) were freshly prepared to a final concentration of 100 mM in absolute ethanol. For each experiment, MS media was freshly prepared and cooled for 1 h in a 55 to 60 °C water bath after autoclaving before adding chemicals.

Cloning and generation of transgenic lines

DNA constructs were created with the Gateway cloning technology (Karimi et al. 2007). The genomic PSY1 sequence and the 1,200 pb PSY1-promoter, including the 5′UTR, were amplified using the primers described in Table S3. These sequences were then recombined with pENTR/D-TOPO (Invitrogen, Cat#45-0218) to yield pTOPO_PSY1 and pTOPO_ProPSY1. The latter vectors were used in a Gateway LR cloning (Gateway LR Clonase II Plus Enzyme Mix, Invitrogen; Cat#12538-120) with pEarleyGate100 (Earley et al. 2006) and pGWB504 (Nakagawa et al. 2007) to yield *Pro35S:PSY1* and *ProPSY1:GFP* constructs. The generated vectors were transferred to *Agrobacterium tumefaciens* strain GV3101, which was used in floral dip transformations. *Pro35S:PSY1* and pEarleyGate100 (EV) transformants were obtained in Col-0, *tt4-11*, *tt5-2*, *tt7-7*, *myb12*, and Col-0 expressing the construct *pCYCB1;1:GFP*. *ProPSY1:GFP* lines were generated in Col-0.

Analysis of root growth

For root elongation measurements, seedlings were grown vertically for 6 to 7 d, depending on the experiment. Starting from day 3 after sowing until the end of the experiment, a dot was drawn at the position of the root tip. Finally, plates were photographed, and the root length was measured over time with Fiji Is Just ImageJ (Schindelin et al. 2012). Root growth rate, expressed in millimeters per hour, was estimated from root length (millimeters) vs. plant age (days after sowing) plots.

Six or 7-d-old seedlings were imaged under a bright field using a Zeiss Discovery 20 equipped with an Axiocam 506 color camera. The picture was taken to highlight the appearance of the first root hair bulge, defined as the first observed root hair in stage +2 (Denninger et al. 2019). In addition, the distance between root hairs was assessed in a continuous file of epidermal trichoblasts cells using Fiji.

Confocal microscopy

Laser scanning confocal microscopy (LSCM) was performed throughout the study using a Plan Apochromat 20×/0.75 CS2 lens on a Leica TCS SP8 microscope. For all the reporter line analyses, roots were stained with 15 μg/mL propidium iodide (PI) (Sigma), rinsed, and mounted in water, except for *pTCSn::GFP*, in which plants were directly mounted without staining. Fluorescence signals were

visualized after excitation by a 488-nm laser line for GFP, YFP, and PI or by a 448-nm laser line for CFP. The fluorescence emission was collected between 600 and 700 nm for PI, 495 and 555 nm for GFP and YFP, and 465 and 570 nm for GFP. Fluorescence intensity measurements for *ProPLT1:CFP* and *ProPLT1:PLT1:YFP* were performed as described in Ercoli et al. (2018). For *ProPSY1:GFP*, *ProCHS:CHS-GFP*, *ProFLS1:FLS1-GFP*, *pTCSn::GFP*, and *DR5v2::n3GFP*, sum intensity projections were generated from 30 z-section images taken in different locations along the root longitudinal axis. After removing the background, the average GFP intensity was measured, and values were expressed as a fold change relative to the control plants. The fluorescence signal was only measured in the stele for the auxin response reporter line *DR5v2::n3GFP*. *pTCSn::GFP* seedlings were 5 d post-germination at the time of the transfer to plates containing either mock or PSY1 synthetic peptide. The gain for GFP acquisition in *ProPSY1:GFP* analysis was set to avoid saturation in the DZ.

For combined cell wall and lignin staining, seedling fixation and staining were performed using an adapted ClearSee protocol (Ursache et al. 2018). Briefly, 6 or 7-d-old seedlings were fixed for 1 h at room temperature in 10% neutral buffered formalin in PBS, using 6-well plates, then washed 5 times for 1 min with PBS 1×. Once fixed, seedlings were cleared in ClearSee solution for at least 24 h under mild shaking. Fixed and cleared samples were incubated overnight in a ClearSee solution supplemented with 0.2% Basic Fuchsin and 0.1% Calcofluor White. After 12 h, the staining solution was removed, and samples were rinsed once in fresh ClearSee solution, then washed twice for at least 120 min in a renewed ClearSee solution with gentle shaking. Roots were carefully placed on a microscope slide with ClearSee and covered with a coverslip. Excitation and detection windows were set as follows: Basic Fuchsin excitation at 552 nm and detection between 600 and 650 nm, Calcofluor white for excitation at 405 nm, and detection between 415 and 570 nm. Central longitudinal section images were acquired to generate a cell length profile by measuring the length of every consecutive cortical cell located from the QC until the DZ for each plant. MZ length is defined as the region of isodiametric cells from the QC up to the cell that was twice the length of the immediately preceding cell and was determined according to the file of cortical cells (Ioio et al. 2008). Mature cortical cell length was assessed in 10 consecutive cells, starting 6 cells above the cortical cell closest to the epidermal cell with the first root hair bulge (Cajero Sánchez et al. 2018).

DPBA staining

We analyzed flavonols accumulation in roots using the probe DPBA as described in (Lewis et al. 2011), which allows for distinct visualization of kaempferol DPBA (K-DPBA) and quercetin DPBA (Q-DPBA) using LSCM. Briefly, individual seedlings were stained in 0.25% w/v DPBA (Sigma-Aldrich), which was dissolved in 0.01% Triton-X (v/v) in water on a rotary shaker at low speed for 7 min. The roots were washed in deionized water for 7 min on the same shaker and mounted in deionized water for imaging. Fluorescence signals were visualized after excitation by a 448 nm laser line, and the emission spectra were captured between 475 to 504 nm for K-DPBA and 577 to 619 nm for Q-DPBA. The specificity of the signal was tested using *tt4-11*, which does not produce flavonols, grown with and without synthetic naringenin, the precursor that *tt4-11* is unable to synthesize (Fig. S9). All the images were acquired using identical settings, except for the laser intensity and digital gain that were increased for imaging in the DZ. To generate the plot profiles in Fig. 4j, in which all developmental zones are imaged together, the gain was set to avoid saturation in the TZ and DZ. Sum intensity projections were generated from about 30 z-section images taken in different locations along the root longitudinal axis. After removing the background, the average intensity of K-DPBA and Q-DPBA was measured, and values were expressed as a fold change relative to the control plants.

ROS detection

ROS quantification was performed as described in Yamada et al. (2020). Briefly, for superoxide anion (O_2^-) quantification, 7-d-old seedlings were stained for 15 min in a solution of 200 μM NBT in 20 mM phosphate buffer (pH 6.1) in the dark and rinsed twice with distilled water. Images for NBT staining were obtained using a 20× objective using a Leica DFC7000 T Camera. The total intensities of NBT staining in the MZ were measured using Fiji (Schindelin et al. 2012). To detect hydrogen peroxide, we incubated 6-d-old seedlings with H_2O_2-3′-O-acetyl-6′O-pentafluorobenzenesulfonyl-2′-7′-difluorofluorescein-Ac (BES-H_2O_2-Ac) (Maeda et al. 2004) (WAKO) 50 μM for 30 min in the dark, then mounted them in 10 mg mL^{-1} PI in water. Roots were observed using a 20× objective with the LSCM. Excitation and detection windows were set as follows: BES-H_2O_2-Ac, excitation at 488 nm and detection at 500 to 550 nm; PI staining, excitation at 488 nm, and detection at 600 to 700 nm. Central longitudinal section images were acquired to quantify BES-H_2O_2-Ac in the root epidermis from the QC until the DZ. The BES-H_2O_2-Ac intensity as a plot profile for fifteen seedlings was generated as described in Ercoli et al. (2018) and averaged for final representation.

Total RNA extraction and library preparation

Col-0 seedlings were grown on a permeable membrane placed on a clear agar MS. Five-days post-germination, seedlings were transferred to a control medium or medium containing PSY1 (50 nM) by moving the membrane to the selected media. After 4 h, the root

tip from each seedling was dissected using an ophthalmic scalpel. For each treatment, 3 replicates of 200 root sections were generated. We extracted total RNA from the samples using Spectrum Plant Total RNA kit (Sigma). RNA samples were treated with DNase I during RNA extraction. RNA quality was examined using a 2100 Bioanalyzer (Agilent). The concentration of total RNA was measured by a Qubit (Invitrogen) instrument. mRNA was isolated from an input of 1,000 ng of total RNA with oligo dT magnetic beads and fragmented to 300 to 400 bp with divalent cations at a high temperature. Using TruSeq stranded mRNA kit (Illumina), the fragmented mRNA was reverse transcribed to create the first strand of cDNA with random hexamers and SuperScript II Reverse Transcriptase (Thermo Fisher Scientific) followed by second strand synthesis. The double-stranded cDNA fragments were treated with A-tailing ligation with JGI's unique dual indexed adapters (IDT) and enriched using 8 cycles of PCR. The prepared libraries were quantified using KAPA Biosystems' next-generation sequencing library qPCR kit and run on a Roche LightCycler 480 real-time PCR instrument. Sequencing of the flowcell was performed on the Illumina NextSeq500 sequencer using NextSeq500 NextSeq HO kits, v2, following a 2×151 indexed run recipe.

Differential expression analysis after PSY1 treatment

Raw fastq file reads were filtered and trimmed using the JGI QC pipeline, resulting in the filtered fastq file (*.filter-RNA.gz files). Using BBDuk (https://sourceforge.net/projects/bbmap/), raw reads were evaluated for artifact sequence by kmer matching (kmer=25), allowing 1 mismatch, and detected artifact was trimmed from the 3′ end of the reads. RNA spike-in reads, PhiX reads, and reads containing any Ns were removed. Quality trimming was performed using the phred trimming method set at Q6. Finally, following trimming, reads under the length threshold were removed (minimum length 25 bases or 1/3 of the original read length—whichever is longer). Filtered reads from each library were aligned to the TAIR10 Arabidopsis genome using HISAT2 version 2.1.0 (Kim et al. 2015). featureCounts (Liao et al. 2014) was used to generate the raw gene counts using gff3 annotations. Only primary hits assigned to the reverse strand were included in the raw gene counts (-s 2 -p --primary options). EdgeR (version 3.30.3) (Robinson et al. 2010) was subsequently used to determine which genes were differentially expressed between pairs of conditions. Genes with a false discovery rate (FDR)-adjusted $P \leq 0.05$ were regarded as differentially expressed between the PSY and mock treatment.

The gene expression data for the longitudinal and radial roots was obtained from (Brady et al. 2007). Genes identified as differentially expressed following PSY1 treatment were mapped to this dataset using their Arabidopsis gene identifiers. An in-house R script was developed to generate heatmaps using the extracted spatial expression values. The script utilized the Elbow and Silhouette methods to determine the appropriate number of clusters. After analyzing the data using both methods, we identified that the optimal number of clusters is 4.

The enriched GO groups among differentially expressed genes were identified using Panther DB (Mi et al. 2019), while the Database for Annotation, Visualization, and Integrated Discovery (DAVID) (Sherman et al. 2022) (https://david.ncifcrf.gov/[AQ11]) was used for the KEGG pathway enrichment analysis. For the comprehensive analysis of single-cell gene expression across specific time zones and cell types (Shahan et al. 2022), expression data was sourced from the Arabidopsis Root Virtual Expression eXplorer (ARVEX), accessible at https://shiny.mdc-berlin.de/ARVEX/. For each gene of interest, data was extracted to pinpoint both the temporal zone and cell type specificity. To determine the average normalized gene expression value, we averaged the expression levels of each gene within the designated time zones and cell types. Furthermore, we quantified the extent of gene expression in each cell population. This was achieved by calculating the proportion of cells expressing a particular gene, which divided the number of cells exhibiting expression by the total cell count. GO, KEGG, and single-cell RNAseq data visualization was performed using a bubble plot generated utilizing the ggplot2 package in RStudio (version 2023.09.1 + 494) with R version 3.3.0+ (Wickham 2016). In the bubble plots for GO and KEGG, the y-axis shows the FDR in a negative Log_{10} scale, whereas the *x*-axis is fixed, and terms from the same KEGG/GO subtree are located closer to each other. The size of each circle represents the term Fold Enrichment in the Log_{10} scale.

Gene expression analysis via RT-qPCR

Total RNA (1 μg) was extracted from whole 7-d-old seedling tissue using TRIzol reagent (Invitrogen) and treated with the TURBO DNA-free kit (Ambion) to remove residual genomic DNA. cDNA was synthesized using the High-Capacity cDNA Reverse Transcription Kit (Applied Biosystems). The cycle threshold (Ct) value was measured on a Bio-Rad CFX96 Real-Time System coupled to a C1000 Thermal Cycler (Bio-Rad) using the iTaq Universal SYBR Green Supermix (Bio-Rad). Normalized relative quantities (NRQs) were obtained using the qBase method (Hellemans et al. 2007), with RPS26E and PAC1 as reference genes for normalization across samples. NRQ values were normalized to the mean value obtained in wt or control (EV) plants. For the synthetic PSY1 time-course experiment, NRQ values were normalized to the mean value obtained in Mock-0 h. NRQ Melting curve analyses at the end of the process and "no template controls" were performed to ensure product-specific amplification without primer–dimer artifacts. Primer sequences are given in Table S3. Three biological replicates were analyzed.

High-resolution mass spectrometry for accurate mass identification of PSY1

Col-0 and *Pro35S:PSY1* seedlings were germinated on ½ MS plates supplemented with 1% (w/v) sucrose. Four-days post-germination, 50 seedlings were transferred into 100 mL of liquid ½ MS medium containing 1% (w/v) sucrose and 25 mM $CaCl_2$, and cultured for 14 d without shaking. Culture medium from 2 independent flasks was collected, filtered through 0.22 μm pore-size membranes to remove particulates, and subsequently lyophilized. The dried medium was then resuspended in 20 mL of 1% (v/v) aqueous N-ethylmorpholine and apoplastic peptides were extracted using o-chlorophenol followed by acetone precipitation as described by Ogawa-Ohnishi and Matsubayashi (2024). The resulting precipitated peptides were solubilized in 50% aqueous acetonitrile using a sonicator water bath and lyophilized again. Peptides were then reconstituted in water, ziptipped, and eluted into 10 μL of 60% aqueous acetonitrile. Peptide samples were then directly infused into a ThermoScientific Q-Exactive HF Orbitrap mass spectrometer and analyzed in the negative ionization mode. Data processing and analysis were conducted using the Qualbrowser application of Xcalibur software (ThermoFisher Scientific).

Arabidopsis root exudate collection

Col-0, *psy1*, *Pro35S:PSY1* and *tt4-11*, seedlings were germinated on MS media, 4-d after germination, 4 biological replicates with 50 to 60 uniformly sized seedlings were selected and transferred onto a sterile, permeable membrane that had been pre-laid on fresh MS medium. For the PSY1-treated samples, Col-0 seedlings were grown on the membrane 2 d before being transferred for 24 h to either a control medium or MS medium supplemented with PSY1 (250 nM) by moving the membrane accordingly. Plants were grown for an additional 3 d on the membrane for the stable line samples. The MS medium associated with the elongation and DZs of the roots was selected to collect root exudates, and a defined rectangular segment measuring 1 cm × 8 cm was excised from the medium. Control samples were generated from plates containing the membrane pre-laid on top of MS media, or MS media supplemented with synthetic PSY1 (250 nM) without plants. This segment was immediately transferred into a pre-weighed 5 mL Eppendorf tube (Catalog #0030119401) to ensure accurate determination of the medium weight. Finally, the collected exudate samples were stored at −80 °C until further analysis.

Liquid chromatography sample preparation

To extract metabolites from media associated with roots and control samples (~2 g agar each), samples were first frozen, lyophilized dry (FreeZone 2.5 Plus; Labconco), then powderized by bead-beating (MiniBeadbeater96, BioSpec) for 5 s, 2×, using a 3.2 mm stainless steel bead. Next, 1.5 mL of 100% methanol was added to each powderized agar sample, briefly vortexed, then sonicated in an iced water bath for 10 min. Samples were centrifuged (5 min, 11,000×*g*) to pellet debris, supernatant removed, and transferred to a 2 mL Eppendorf, dried in a SpeedVac (SPD111V; Thermo Fisher Scientific). Next, 1 mL of 100% methanol was added to each dried extract, briefly vortexed, then sonicated in an iced water bath for 10 min. Samples were centrifuged again, then supernatant removed and transferred to a 2 mL Eppendorf and dried in a SpeedVac. All dried extracts were stored frozen at −80 °C. The same extraction procedures were followed using empty 5 mL tubes and 2 mL tubes containing synthetic PSY1 (100 nM) to serve as extraction controls (5 replicates each). In preparation for LC-MS, samples were resuspended in 150 μL of 100% methanol containing a mix of isotopically labeled internal standards.

LC-MS/MS untargeted metabolomics analysis

Samples were run using both normal and reverse phase chromatography. Each of these was performed using an Agilent 1290 LC stack, with MS and MS/MS data collected using an Exploris 120 Orbitrap MS (Thermo Fisher Scientific, San Jose, CA, USA) for normal phase, and QExactive HF Orbitrap for reverse phase. Mass spectrometer parameters and gradients are provided in this protocols.io (dx.doi.org/10.17504/protocols.io.kxygxydwkl8j/v1) for normal phase, and this protocols.io (dx.doi.org/10.17504/protocols.io.ewov19r27lr2/v1) for reverse phase. For both normal phase and reverse phase, full MS1 spectra was collected at 60k resolution in both positive and negative ionization mode, with MS/MS fragmentation data acquired using stepped then averaged 10, 20, and 40 eV collision energies at 15k resolution. For normal phase, the MS1 m/z range for data collection was 70 to 1,050, while for reverse phase, both m/z 80 to 1,200 and m/z 1,000 to 3,000 were used in separate runs to cover mass ranges for metabolites and peptides. Samples consisted of 4 biological replicates each and 5 biological replicates for the extraction controls, with sample injection order randomized by replicate and an injection blank of 100% methanol run between each sample, with the blank replaced by an injection of internal standard mix every third sample, as well as QC mix every 15 samples. The raw data from the metabolite LC-MS runs are provided in Data Set S5. For untargeted data analysis, features with 0.8 min < RT < 18.5 min (polar/HILIC-Z chromatography) and features with 0.5 min < RT < 9.5 min (nonpolar/C18 chromatography), and a maximum peak height fold-change between sample and extraction controls and MS media samples >4 were selected. For samples in which features were not detected, we replaced 0 values with ⅔ of the smallest non-zero value to avoid errors when dividing by 0. We performed a

Feature-Based Molecular Networking (FBMN) (Nothias et al. 2020) workflow using MZmine-3.7. (Schmid et al. 2023) and Global Natural Products Social Molecular Networking (GNPS2; http://gnps2.org) (Wang et al. 2016). The MZmine workflow was used to generate a list of features obtained from extracted ion chromatograms containing chromatographic peaks within a narrow m/z range and filtered to remove isotopes. For each feature, the most intense fragmentation spectrum was uploaded to GNPS for putative identification by comparison with mass spectra deposited in the database. We accepted top GNPS annotations with cosine scores of MS/MS spectral mirror match (MQScore) to library reference of >0.7 (67 features) (Data Set S6). PCA was performed on $\log_{10}$-transformed data with scaling enabled; the variance explained by the first 2 principal components (PC1 and PC2) was calculated, and the resulting PCA scores were merged with the corresponding sample metadata. Euclidean distances were then computed on the scaled, $\log_{10}$-transformed filtered data, and a permutational multivariate analysis of variance (PERMANOVA) was conducted using adonis2 (999 permutations) to assess differences between conditions (Oksanen et al. 2001). We calculated the average peak height fold change for each feature (PSY1 treatment vs. mock, or for stables mutant and overexpression lines compared with Col-0 wt). Using Cytoscape software, we conducted feature-based molecular networking. Flavonoids were identified using the compound classes attributed to identified compounds using NPClassifier (Kim et al. 2021).

For targeted analysis, compound identification was performed by comparing detected m/z, retention time (RT) and fragmentation pattern to standards run in-house using the same LC-MS methods and assigning a confidence level based on these criteria (Data Sets S9 and S10. For each identified compound, the highest level of confidence (Exceeds Level 1) (Sumner et al. 2007)was achieved when the measured m/z agreed with the expected theoretical m/z with <5 ppm error, detected RT of the feature was within 0.5 min of theoretical, and fragmentation pattern matched that of the standard. When MSMS was not collected, some compounds were identified based on only mz and RT (Level 1); mis-matching MSMS would invalidate an identification.

Statistical analysis

Statistical analysis was performed using GraphPad Prism 9 (GraphPad Software). The specific statistical tests ran are specified in the figure legends. Differences were considered to be significant when $P < 0.05$. The detailed statistical analysis data are shown in Data Set S11.

Accession numbers

Accession numbers for the major genes and proteins analyzed in this study are listed in Fig. 3b and in Tables S1 and S3.

Acknowledgments

We thank Jorge Dubcovsky for the use of the Zeiss stereoscope; Ben Scheres for the *ProPLT1-CFP* and *ProPLT1:PLT1-YFP* reporters; Gloria Muday for the *ProCHS:CHS-GFP* reporter; Christoph Ringli for the *ProFLS1:FLS1-GFP* reporter; Wolfgang Busch for the *DR5v2:3nGFP* reporter; Cris Argueso for the p*TCSn::GFP* reporter, Peter Doener for the *ProCYCB1;1:CYCB1;1-GFP* reporter, Shahid Siddique for the triple PSY receptor mutant, Audrey Adamchak, Rory Greenhalgh, and Ryan Packer for their invaluable help; Ellen Youngsoo Rim, Valley Stewart, Dee Dee Luu, Wolfgang Busch and Ramiro E. Rodriguez for the comments on the manuscript.

Author contributions

Conceptualization: M.F.E. and P.C.R. Methodology: M.F.E., A.M.S., A.T.A., K.B.L., B.P.B., T.S.W., S.R., R.J., T.R.N., and P.C.R. Investigation: M.F.E., A.M.S., A.T.A., K.B.L., B.P.B., T.S.W., S.R., R.J., T.R.N., and P.C.R. Visualization: M.F.E. and P.C.R. Supervision: P.C.R. Writing—original draft: M.F.E. and P.C.R. Writing—review & editing: M.F.E., A.M.S., A.T.A., K.B.L., B.P.B., T.S.W., S.R., R.J., T.R.N., and P.C.R.

Supplementary material[AQ38]

Supplementary material is available at *The Plant Cell* online.

Funding

[AQ12]M.F.E. is a 2019 Latin American Fellow in the Biomedical Sciences supported by the Pew Charitable Trusts. A.M.S. is a USDA-NIFA-AFRI Postdoctoral Fellow (2023-67012-39889). The Innovative Genomics Institute (IGI), funded by the Chan Zuckerberg Initiative. The National Institutes of Health (GM148173). The Joint BioEenergy Institute[AQ13], supportedfunded by the US Department of Energy, Office of Science, Biological and Environmental Research Program, through contract fo. DE-AC02-05CH11231)between Lawrence Berkeley National Laboratory and the U.S. Department of Energy. The RNA-seq analysis and the metabolomic analysis (proposal: https://doi.org/10.46936/10.25585/60000897) was conducted by the U.S. Department

of Energy Joint Genome Institute, a DOE Office of Science User Facility, supported by the Office of Science of the U.S. Department of Energy operated under Contract No. DE-AC02-05CH11231. The United States Government retains and the publisher, by accepting the article for publication, acknowledges that the United States Government retains a nonexclusive, paid-up, irrevocable, worldwide license to publish or reproduce the published form of this manuscript, or allow others to do so, for United States Government purposes. Any subjective views or opinions that might be expressed in this paper do not necessarily represent the views of the U.S. Department of Energy or the United States Government. National Institutes of Health Administrative Supplements for the purchase of the Confocal Microscope Leica SP8 (grant no. GM122968) and the ThermoScientific Q-Exactive HF Orbitrap mass spectrometer (grant no. 1S10OD025271-01A1).

Conflicts of interest[AQ14]

~~T.R.N. is an advisor to Brightseed Bio.~~ T.R.N. is a founder of two non-profits, Prosper Soils and Bioaligned Labs with prior approval fr om LBNL. The remaining authors declare no competing interests.

Conflict of interest statement,

T.R.N. is a founder of two non-profits, Prosper Soils and Bioaligned Labs with prior approval from LBNL. The remaining authors decla re no competing interests.

Data availability

All data are available in the main text or the Supplementary Materials. The raw data for RNA sequencing are available in the Sequence Read Archive database under BioProject PRJNA616620, PRJNA616621, PRJNA616622, PRJNA616623, PRJNA616551, PRJNA616552. A previous version of this work was deposited in the preprint depository server bioRxiv. All code from this study is available upon request. The metabolomic raw data can be accessed at Massive repository (MSV000098293).

References[AQ15]

Agati G, Azzarello E, Pollastri S, Tattini M. 2012. Flavonoids as antioxidants in plants: location and functional significance. Plant Sci. 196:67–76. https://doi.org/10.1016/j.plantsci.2012.07.014.

Aghdam MS, Sayyari M, Luo Z. 2021. Exogenous phytosulfokine α application delays senescence and promotes antioxidant nutrient accumulation in strawberry fruit during cold storage by triggering endogenous phytosulfokine α signaling. Postharvest Biol Technol. 175:111473. https://doi.org/10.1016/j.postharvbio.2021.111473.

Aida M et al. 2004. The PLETHORA genes mediate patterning of the Arabidopsis root stem cell niche. Cell. 119:109–120. https://doi.org/10.1016/j.cell.2004.09.018.

Amano Y, Tsubouchi H, Shinohara H, Ogawa M, Matsubayashi Y. 2007. Tyrosine-sulfated glycopeptide involved in cellular proliferation and expansion in Arabidopsis. Proc Natl Acad Sci U S A. 104:18333–18338. https://doi.org/10.1073/pnas.0706403104.

Appelhagen I et al. 2014. Update on transparent testa mutants from *Arabidopsis thaliana*: characterisation of new alleles from an isogenic collection. Planta. 240:955–970. https://doi.org/10.1007/s00425-014-2088-0.

Barbez E, Dünser K, Gaidora A, Lendl T, Busch W. 2017. Auxin steers root cell expansion via apoplastic pH regulation in *Arabidopsis thaliana*. Proc Natl Acad Sci U S A. 114:E4884–E4893. https://doi.org/10.1073/pnas.1613499114.

Beemster GTS, Baskin TI. 1998. Analysis of cell division and elongation underlying the developmental acceleration of root growth in *Arabidopsis thaliana*. Plant Physiol. 116:1515–1526. https://doi.org/10.1104/pp.116.4.1515.

Blilou I et al. 2005. The PIN auxin efflux facilitator network controls growth and patterning in Arabidopsis roots. Nature. 433:39–44. https://doi.org/10.1038/nature03184.

Brady SM et al. 2007. A high-resolution root spatiotemporal map reveals dominant expression patterns. Science. 318:801–806. https://doi.org/10.1126/science.1146265.

Brown DE et al. 2001. Flavonoids act as negative regulators of auxin transport in vivo in Arabidopsis. Plant Physiol. 126:524–535. https://doi.org/10.1104/pp.126.2.524.

Brunetti C, Fini A, Sebastiani F, Gori A, Tattini M. 2018. Modulation of phytohormone signaling: a primary function of flavonoids in plant–environment interactions. Front Plant Sci. 9:1042. https://doi.org/10.3389/fpls.2018.01042.

Buer CS, Djordjevic MA. 2009. Architectural phenotypes in the transparent testa mutants of *Arabidopsis thaliana*. J Exp Bot. 60:751–763. https://doi.org/10.1093/jxb/ern323.

Bühler E, Fahrbach E, Schaller A, Stührwohldt N. 2023. Sulfo-peptide CLEL6 inhibits anthocyanin biosynthesis in *Arabidopsis thaliana*. Plant Physiol. 193:809–820. https://doi.org/10.1093/plphys/kiad316.

Cajero Sánchez W, García-Ponce B, Sánchez MP, Álvarez-Buylla ER, Garay-Arroyo A. 2018. Identifying the transition to the maturation zone in three ecotypes of *Arabidopsis thaliana* roots. Commun Integr Biol. 11:e1395993. https://doi.org/10.1080/19420889.2017.1395993.

Daryanavard H, Postiglione AE, Mühlemann JK, Muday GK. 2023. Flavonols modulate plant development, signaling, and stress responses. Curr Opin Plant Biol. 72:102350. https://doi.org/10.1016/j.pbi.2023.102350.

De Giorgi J et al. 2021. The Arabidopsis mature endosperm promotes seedling cuticle formation via release of sulfated peptides. Dev Cell. 56:3066–3081.e5. https://doi.org/10.1016/j.devcel.2021.10.005.

Denninger P et al. 2019. Distinct RopGEFs successively drive polarization and outgrowth of root hairs. Curr Biol. 29:1854–1865.e5. https://doi.org/10.1016/j.cub.2019.04.059.

Di Mambro R et al. 2017. Auxin minimum triggers the developmental switch from cell division to cell differentiation in the Arabidopsis root. Proc Natl Acad Sci U S A. 114:E7641–E7649. https://doi.org/10.1073/pnas.1705833114.

Earley KW et al. 2006. Gateway-compatible vectors for plant functional genomics and proteomics. Plant J. 45:616–629. https://doi.org/10.1111/j.1365-313X.2005.02617.x.

Ercoli MF, Vena R, Goldy C, Palatnik JF, Rodríguez RE. 2018. Analysis of expression gradients of developmental regulators in *Arabidopsis thaliana* roots. Methods Mol Biol. 1863:3–17. https://doi.org/10.1007/978-1-4939-8772-6_1.

Ercoli MF et al. 2022. Plant immunity: rice XA21-mediated resistance to bacterial infection. Proc Natl Acad Sci U S A. 119:e2121568119. https://doi.org/10.1073/pnas.2121568119.

Galinha C et al. 2007. PLETHORA proteins as dose-dependent master regulators of Arabidopsis root development. Nature. 449:1053–1057. https://doi.org/10.1038/nature06206.

Gayomba SR, Muday GK. 2020. Flavonols regulate root hair development by modulating accumulation of reactive oxygen species in the root epidermis. Development. 147:dev185819. https://doi.org/10.1242/dev.185819.

Grunewald W et al. 2012. Transcription factor WRKY23 assists auxin distribution patterns during Arabidopsis root development through local control on flavonol biosynthesis. Proc Natl Acad Sci U S A. 109:1554–1559. https://doi.org/10.1073/pnas.1121134109.

Hellemans J, Mortier G, De Paepe A, Speleman F, Vandesompele J. 2007. Qbase relative quantification framework and software for management and automated analysis of real-time quantitative PCR data. Genome Biol. 8:R19. https://doi.org/10.1186/gb-2007-8-2-r19.

Heyman J, Kumpf RP, De Veylder L. 2014. A quiescent path to plant longevity. Trends Cell Biol. 24:443–448. https://doi.org/10.1016/j.tcb.2014.03.004.

Hsiao Y-C, Yamada M. 2021. The roles of peptide hormones and their receptors during plant root development. Genes (Basel). 12:22. https://doi.org/10.3390/genes12010022.

Ioio RD et al. 2008. A genetic framework for the control of cell division and differentiation in the root meristem. Science. 322:1380–1384. https://doi.org/10.1126/science.1164147.

Ivanov VB, Dubrovsky JG. 2013. Longitudinal zonation pattern in plant roots: conflicts and solutions. Trends Plant Sci. 18:237–243. https://doi.org/10.1016/j.tplants.2012.10.002.

Jackson D, Roberts K, Martin C. 1992. Temporal and spatial control of expression of anthocyanin biosynthetic genes in developing flowers of Antirrhinum majus. Plant J. 2:425–434. https://doi.org/10.1111/j.1365-313X.1992.00425.x.

Karimi M, Depicker A, Hilson P. 2007. Recombinational cloning with plant gateway vectors. Plant Physiol. 145:1144–1154. https://doi.org/10.1104/pp.107.106989.

Kaufmann C, Sauter M. 2019. Sulfated plant peptide hormones. J Exp Bot. 70:4267–4277. https://doi.org/10.1093/jxb/erz292.

Kim D, Langmead B, Salzberg SL. 2015. HISAT: a fast spliced aligner with low memory requirements. Nat Methods. 12:357–360. https://doi.org/10.1038/nmeth.3317.

Kim HW et al. 2021. NPClassifier: a deep neural network-based structural classification tool for natural products. J Nat Prod. 84:2795–2807. https://doi.org/10.1021/acs.jnatprod.1c00399.

Komori R, Amano Y, Ogawa-Ohnishi M, Matsubayashi Y. 2009. Identification of tyrosylprotein sulfotransferase in Arabidopsis. Proc Natl Acad Sci U S A. 106:15067–15072. https://doi.org/10.1073/pnas.0902801106.

Koornneef M. 1990. Mutations affecting the testa colour in Arabidopsis. Arabidopsis Information Service. 27. p. 1–4.

Le J, Vandenbussche F, Van Der Straeten D, Verbelen JP. 2004. Position and cell type-dependent microtubule reorientation characterizes the early response of the Arabidopsis root epidermis to ethylene. Physiol Plant. 121:513–519. https://doi.org/10.1111/j.1399-3054.2004.00342.x.

~~Lee D et al. 2020. Regulation of reactive oxygen species during plant immunity through phosphorylation and ubiquitination of RBOHD. Nat Commun. 11:1838. https://doi.org/10.1038/s41467-020-15601-5.[AQ16]~~

Lewis DR et al. 2011. Auxin and ethylene induce flavonol accumulation through distinct transcriptional networks. Plant Physiol. 156:144–164. https://doi.org/10.1104/pp.111.172502.

Li M et al. 2022. Brassinosteroid signaling restricts root lignification by antagonizing SHORT-ROOT function in Arabidopsis. Plant Physiol. 190:1182–1198. https://doi.org/10.1093/plphys/kiac327.

Liao C-Y et al. 2015. Reporters for sensitive and quantitative measurement of auxin response. Nat Methods. 12:207–210. https://doi.org/10.1038/nmeth.3279.

Liao Y, Smyth GK, Shi W. 2014. featureCounts: an efficient general purpose program for assigning sequence reads to genomic features. Bioinformatics. 30:923–930. https://doi.org/10.1093/bioinformatics/btt656.

Liu J, Müller B. 2017. Imaging TCSn::GFP, a synthetic cytokinin reporter, in *Arabidopsis thaliana*. Methods Mol Biol. 1497:81–90. https://doi.org/10.1007/978-1-4939-6469-7_9.

Liu S et al. 2022. Cytokinin promotes growth cessation in the Arabidopsis root. Curr Biol. 32:1974–1985.e3. https://doi.org/10.1016/j.cub.2022.03.019.

Luo X, Chen Z, Gao J, Gong Z. 2014. Abscisic acid inhibits root growth in Arabidopsis through ethylene biosynthesis. Plant J. 79:44–55. https://doi.org/10.1111/tpj.12534.

Maeda H et al. 2004. Fluorescent probes for hydrogen peroxide based on a non-oxidative mechanism. Angew Chem Int Ed Engl. 43:2389–2391. https://doi.org/10.1002/anie.200452381.

Mähönen AP et al. 2014. PLETHORA gradient formation mechanism separates auxin responses. Nature. 515:125–129. https://doi.org/10.1038/nature13663.

Markakis MN et al. 2012. Identification of genes involved in the ACC-mediated control of root cell elongation in *Arabidopsis thaliana*. BMC Plant Biol. 12:208. https://doi.org/10.1186/1471-2229-12-208.

Matsubayashi Y. 2014. Posttranslationally modified small-peptide signals in plants. Annu Rev Plant Biol. 65:385–413. https://doi.org/10.1146/annurev-arplant-050312-120122.

Matsuzaki Y, Ogawa-Ohnishi M, Mori A, Matsubayashi Y. 2010. Secreted peptide signals required for maintenance of root stem cell niche in Arabidopsis. Science. 329:1065–1067. https://doi.org/10.1126/science.1191132.

Mehrtens F, Kranz H, Bednarek P, Weisshaar B. 2005. The Arabidopsis transcription factor MYB12 is a flavonol-specific regulator of phenylpropanoid biosynthesis. Plant Physiol. 138:1083–1096. https://doi.org/10.1104/pp.104.058032.

Mi H et al. 2019. Protocol update for large-scale genome and gene function analysis with the PANTHER classification system (v.14.0). Nat Protoc. 14:703–721. https://doi.org/10.1038/s41596-019-0128-8.

Montesinos JC et al. 2020. Phytohormone cytokinin guides microtubule dynamics during cell progression from proliferative to differentiated stage. EMBO J. 39:e104238. https://doi.org/10.15252/embj.2019104238.

Naik J et al. 2024. Flavonols affect the interrelated glucosinolate and camalexin biosynthetic pathways in *Arabidopsis thaliana*. J Exp Bot. 75:219–240. https://doi.org/10.1093/jxb/erad391.

Nakagawa T et al. 2007. Improved gateway binary vectors: high-performance vectors for creation of fusion constructs in transgenic analysis of plants. Biosci Biotechnol Biochem. 71:2095–2100. https://doi.org/10.1271/bbb.70216.

Nothias L-F et al. 2020. Feature-based molecular networking in the GNPS analysis environment. Nat Methods. 17:905–908. https://doi.org/10.1038/s41592-020-0933-6.

Ogawa-Ohnishi M et al. 2022. Peptide ligand-mediated trade-off between plant growth and stress response. Science. 378:175–180. https://doi.org/10.1126/science.abq5735.

Ogawa-Ohnishi M, Matsubayashi Y. 2024. Extraction of apoplastic peptides for the structural elucidation of mature peptide hormones in Arabidopsis. Methods Mol Biol. 2731:81–87. https://doi.org/10.1007/978-1-0716-3511-7_6.

Oksanen J et al. 2001. vegan: community ecology package. Version 2:7-2. https://doi.org/10.32614/CRAN.package.vegan.

Ou Y et al. 2016. RGF1 INSENSITIVE 1 to 5, a group of LRR receptor-like kinases, are essential for the perception of root meristem growth factor 1 in *Arabidopsis thaliana*. Cell Res. 26:686–698. https://doi.org/10.1038/cr.2016.63.

Pasternak T, Palme K, Pérez-Pérez JM. 2023. Role of reactive oxygen species in the modulation of auxin flux and root development in *Arabidopsis thaliana*. Plant J. 114:83–95. https://doi.org/10.1111/tpj.16118.

Peer WA et al. 2001. Flavonoid accumulation patterns of transparent testa mutants of Arabidopsis. Plant Physiol. 126:536–548. https://doi.org/10.1104/pp.126.2.536.

Peer WA et al. 2004. Variation in expression and protein localization of the PIN family of auxin efflux facilitator proteins in flavonoid mutants with altered auxin transport in *Arabidopsis thaliana*. Plant Cell. 16:1898–1911. https://doi.org/10.1105/tpc.021501.

Perez de Souza L, Garbowicz K, Brotman Y, Tohge T, Fernie AR. 2020. The acetate pathway supports flavonoid and lipid biosynthesis in Arabidopsis. Plant Physiol. 182:857–869. https://doi.org/10.1104/pp.19.00683.

~~Pruitt RN et al. 2015. The rice immune receptor XA21 recognizes a tyrosine-sulfated protein from a Gram-negative bacterium. Sci Adv. 1:e1500245. https://doi.org/10.1126/sciadv.1500245.[AQ17]~~

Pruitt RN et al. 2017. A microbially derived tyrosine-sulfated peptide mimics a plant peptide hormone. New Phytol. 215:725–736. https://doi.org/10.1111/nph.14609.

Ringli C et al. 2008. The modified flavonol glycosylation profile in the Arabidopsis rol1 mutants results in alterations in plant growth and cell shape formation. Plant Cell. 20:1470–1481. https://doi.org/10.1105/tpc.107.053249.

Robinson MD, McCarthy DJ, Smyth GK. 2010. edgeR: a Bioconductor package for differential expression analysis of digital gene expression data. Bioinformatics. 26:139–140. https://doi.org/10.1093/bioinformatics/btp616.

Růžička K, Ursache R, Hejátko J, Helariutta Y. 2015. Xylem development—from the cradle to the grave. New Phytol. 207:519–535. https://doi.org/10.1111/nph.13383.

Saito K et al. 2013. The flavonoid biosynthetic pathway in Arabidopsis: structural and genetic diversity. Plant Physiol Biochem. 72:21–34. https://doi.org/10.1016/j.plaphy.2013.02.001.

Salvi E, Di Mambro R, Sabatini S. 2020a. Dissecting mechanisms in root growth from the transition zone perspective. J Exp Bot. 71:2390–2396. https://doi.org/10.1093/jxb/eraa079.

Salvi E et al. 2020b. A self-organized PLT/auxin/ARR-B network controls the dynamics of root zonation development in *Arabidopsis thaliana*. Dev Cell. 53:431–443.e23. https://doi.org/10.1016/j.devcel.2020.04.004.

Saslowsky DE, Dana CD, Winkel-Shirley B. 2000. An allelic series for the chalcone synthase locus in *Arabidopsis*. Gene. 255:127–138. https://doi.org/10.1016/S0378-1119(00)00304-8.

Scheres B, Benfey P, Dolan L. 2002. Root development. Arabidopsis Book. 1:e0101. https://doi.org/10.1199/tab.0101.

Schindelin J et al. 2012. Fiji: an open-source platform for biological-image analysis. Nat Methods. 9:676–682. https://doi.org/10.1038/nmeth.2019.

Schmid R et al. 2023. Integrative analysis of multimodal mass spectrometry data in MZmine 3. Nat Biotechnol. 41:447–449. https://doi.org/10.1038/s41587-023-01690-2.

Serre NB et al. 2023. The AUX1-AFB1-CNGC14 module establishes a longitudinal root surface pH profile. eLife. 12:e85193. https://doi.org/10.7554/eLife.85193.

Shahan R et al. 2022. A single-cell Arabidopsis root atlas reveals developmental trajectories in wild-type and cell identity mutants. Dev Cell. 57:543–560.e9. https://doi.org/10.1016/j.devcel.2022.01.008.

Sherman BT et al. 2022. DAVID: a web server for functional enrichment analysis and functional annotation of gene lists (2021 update). Nucleic Acids Res. 50:W216–W221. https://doi.org/10.1093/nar/gkac194.

Shi L-D et al. 2026. Reduced methane emissions in transgenic rice genotypes are associated with altered rhizosphere microbial hydrogen cycling. Nat Commun. 17:2028. https://doi.org/10.1038/s41467-026-68640-9.

Shinohara H, Mori A, Yasue N, Sumida K, Matsubayashi Y. 2016. Identification of three LRR-RKs involved in perception of root meristem growth factor in Arabidopsis. Proc Natl Acad Sci U S A. 113:3897–3902. https://doi.org/10.1073/pnas.1522639113.

Silva-Navas J et al. 2016. Flavonols mediate root phototropism and growth through regulation of proliferation-to-differentiation transition. Plant Cell. 28:1372–1387. https://doi.org/10.1105/tpc.15.00857.

Somssich M, Khan GA, Persson S. 2016. Cell wall heterogeneity in root development of Arabidopsis. Front Plant Sci. 7:1242. https://doi.org/10.3389/fpls.2016.01242.

Song W et al. 2016. Signature motif-guided identification of receptors for peptide hormones essential for root meristem growth. Cell Res. 26:674–685. https://doi.org/10.1038/cr.2016.62.

Stewart V, Ronald PC. 2022. Sulfotyrosine residues: interaction specificity determinants for extracellular protein–protein interactions. J Biol Chem. 298:102232. https://doi.org/10.1016/j.jbc.2022.102232.

Stracke R et al. 2007. Differential regulation of closely related R2R3-MYB transcription factors controls flavonol accumulation in different parts of the *Arabidopsis thaliana* seedling. Plant J. 50:660–677. https://doi.org/10.1111/j.1365-313X.2007.03078.x.

Stracke R et al. 2010. Analysis of PRODUCTION OF FLAVONOL GLYCOSIDES-dependent flavonol glycoside accumulation in *Arabidopsis thaliana* plants reveals MYB11-, MYB12- and MYB111-independent flavonol glycoside accumulation. New Phytol. 188:985–1000. https://doi.org/10.1111/j.1469-8137.2010.03421.x.

Street IH et al. 2016. Cytokinin acts through the auxin influx carrier AUX1 to regulate cell elongation in the root. Development. 143:3982–3993. https://doi.org/10.1242/dev.132035.

Sumner LW et al. 2007. Proposed minimum reporting standards for chemical analysis chemical analysis working group (CAWG) metabolomics standards initiative (MSI). Metabolomics. 3:211–221. https://doi.org/10.1007/s11306-007-0082-2.

Svolacchia N, Salvi E, Sabatini S. 2020. Arabidopsis primary root growth: let it grow, can't hold it back anymore! Curr Opin Plant Biol. 57:133–141. https://doi.org/10.1016/j.pbi.2020.08.005.

Taylor LP, Grotewold E. 2005. Flavonoids as developmental regulators. Curr Opin Plant Biol. 8:317–323. https://doi.org/10.1016/j.pbi.2005.03.005.

Teale WD et al. 2021. Flavonol-mediated stabilization of PIN efflux complexes regulates polar auxin transport. EMBO J. 40:e104416. https://doi.org/10.15252/embj.2020104416.

Thompson EP, Wilkins C, Demidchik V, Davies JM, Glover BJ. 2010. An Arabidopsis flavonoid transporter is required for anther dehiscence and pollen development. J Exp Bot. 61:439–451. https://doi.org/10.1093/jxb/erp312.

Ursache R, Andersen TG, Marhavý P, Geldner N. 2018. A protocol for combining fluorescent proteins with histological stains for diverse cell wall components. Plant J. 93:399–412. https://doi.org/10.1111/tpj.13784.

Wang J et al. 2015. Allosteric receptor activation by the plant peptide hormone phytosulfokine. Nature. 525:265–268. https://doi.org/10.1038/nature14858.

Wang M et al. 2016. Sharing and community curation of mass spectrometry data with global natural products social molecular networking. Nat Biotechnol. 34:828–837. https://doi.org/10.1038/nbt.3597.

Wang Y, Chen W, Ou Y, Zhu Y, Li J. 2022. Arabidopsis ROOT ELONGATION RECEPTOR KINASES negatively regulate root growth putatively via altering cell wall remodeling gene expression. J Integr Plant Biol. 64:1502–1513. https://doi.org/10.1111/jipb.13282.

Wickham H. 2016. ggplot2. Springer International Publishing.

Xie D-Y, Sharma SB, Wright E, Wang Z-Y, Dixon RA. 2006. Metabolic engineering of proanthocyanidins through co-expression of anthocyanidin reductase and the PAP1 MYB transcription factor. Plant J. 45:895–907. https://doi.org/10.1111/j.1365-313X.2006.02655.x.

Yamada M, Han X, Benfey PN. 2020. RGF1 controls root meristem size through ROS signalling. Nature. 577:85–88. https://doi.org/10.1038/s41586-019-1819-6.

Yonekura-Sakakibara K et al. 2008. Comprehensive flavonol profiling and transcriptome coexpression analysis leading to decoding gene–metabolite correlations in Arabidopsis. Plant Cell. 20:2160–2176. https://doi.org/10.1105/tpc.108.058040.

Žádníková P, Simon R. 2014. How boundaries control plant development. Curr Opin Plant Biol. 17:116–125. https://doi.org/10.1016/j.pbi.2013.11.013.

Zhao Y et al. 2018. Arabidopsis duodecuple mutant of PYL ABA receptors reveals PYL repression of ABA-independent SnRK2 activity. Cell Rep. 23:3340–3351.e5. https://doi.org/10.1016/j.celrep.2018.05.044.

Zluhan-Martínez E et al. 2021. Integrative roles of phytohormones on cell proliferation, elongation and differentiation in the *Arabidopsis thaliana* Primary Root. Front Plant Sci. 12:659155. https://doi.org/10.3389/fpls.2021.659155.